Bell Aerospace TEXTRON
Division of Textron Inc.

Post Office Box One Buffalo, New York 14240

FINAL REPORT
SATELLITE BORNE GRAVITY GRADIOMETER STUDY

CONTRACT NAS 5-20910

NASA GODDARD SPACE FLIGHT CENTER

E.H. Metzger
A. Jircitano
C. Affleck

Report No. 6413-950001

March 1976

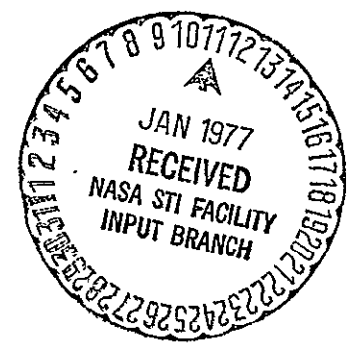

CONTENTS

ILLUSTRATIONS

TABLES

1.0 INTRODUCTION

This document is the final report covering the Satellite Borne Gravity Gradiometer Study conducted by Bell Aerospace under Contract NAS 5-20910 to Goddard Space Flight Center.

A number of earth orbital gravity measuring techniques have been studied and conducted in the past. Satellite-to-satellite doppler velocity measurements and ground tracking of satellite orbital perturbations have successfully yielded the long wave length gravity anomalies of the earth. These techniques give useful gravity anomaly data below the 20th harmonic degree but little information at the higher ones because the orbital perturbations are related to the gravity anomalies through an integration process.

Orbital gravity gradient measurements on the other hand are related to the gravity anomalies through spatial differentiation. Even though the gravity gradients are very much attenuated at orbital altitudes, the analysis discussed in Section 2.0 of this report shows that gravity anomaly determination to the 100th harmonic degree is possible with an orbital gravity gradiometer in the 0.03 EU (10 sec avg. time) (1 Eotvos Unit = 10^{-9} /sec^2) performance category.

Gravity gradiometry is recognized to be a very difficult instrumentation problem because extremely small differential acceleration levels have to be measured, 0.1 EU corresponds to an acceleration of 10^{-11}g at two points 1 meter apart. Bell Aerospace is under contract to SAMSO USAF since April of 1974 to develop a feasibility model of a gravity gradiometer for airborne applications using four modified versions of the proven Model VII accelerometers mounted on a slowly rotating fixture. It is an objective of the program to demonstrate gravity gradient measurements to an accuracy of 1 EU in a ten second time period in all orientations with respect to the g vector and under moving base conditions in the laboratory. The progress so far has been excellent and gravity gradients are being measured to 1.07 EU in a vertical rotation axis orientation. Equally significant are the outstanding operational characteristics such as fast reaction time, low temperature coefficients and high degree of bias stability over long periods of time. The rotating accelerometer gravity gradiometer approach and its present status is discussed in Section 4.0 and is the foundation for the orbital gravity gradiometer analyzed in this report. The performance levels achieved at this time, in a 1 g enviornment of the earth and under relatively high seismic disturbances, lend the orbital gravity gradiometer a high confidence level of success.

A slowly rotating satellite (0.5 to 0.1 rad/sec spin speed) at an altitude of between 250 and 350 km would be an almost ideal vehicle for a gravity gradiometer. The low g and vibration free environment and the "smooth rotation" provided by a spinning vehicle will eliminate many of the error mechanisms present in the airborne gravity gradiometer. Furthermore the low g environment will permit the use of the Space qualified MESA (Miniature Electrostatic Accelerometer) with the inherent lower noise. The electrostatic suspension system of the MESA system provides near zero spring constant along the sensitive axis and eliminated one of the major noise producing sources stemming from the spring suspension of the Model VII proof mass. Over 50 MESAs have successfully operated on various orbital missions including:

No. of Missions	Name	No. of MESAs per Mission
1	Logacs - Agena	1
2	Cannonball Satellite	3
1	Spades	1
7	Agena 110	1
1	SERT II Satellite	1
1	S-73-5 Satellite	1
3	Atmospheric Explorers	3
3	DMA - 501 Experiment	1 three axis MESA

The only modification contemplated to the MESA for the orbital gravity gradiometer application is hard evacuation of the instrument to eliminate gas damping. Hard evacuation was successfully carried out on the Model VII accelerometers and has been maintained for over a year on five instruments.

This report is organized into sections which develop a logical case for an orbital gravity gradiometer.

The analytical section covers a discussion of:

(1) The statistical nature of the gravity anomalies expected to be encountered at an orbital altitude of 300 km and their relationship to gravity gradient anomalies.

(2) An estimation of accuracy with which the gravity anomalies will be measured as a function of gravity gradiometer performance and harmonic degree of the earth.

(3) An estimation of the accuracy with which the gravity anomalies will be measured as a function of satellite tracking accuracy and harmonic degree of the earth.

A descriptive design section of the orbital gravity gradiometer which covers:

(1) The description of the rotating accelerometer orbital gravity gradiometer outlining the techniques of this concept which permits high accuracy gravity gradient measurements with proven and qualified instruments.

(2) A description of the Miniature Electrostatic Accelerometer

(3) Discussion of MESA instrument noise and recommended modifications to reduce it to required level

(4) Discussion of orbital vehicle induced noise and outlining orbital vehicle critical design parameters for the gravity gradiometer mission

(5) A status report of the airborne rotating accelerometer gravity gradiometer development program, which forms the basis for the orbital gravity gradiometer

(6) Short section summarizing the conclusions and recommendations.

2.0 DISCUSSION AND ANALYSIS OF ORBITAL GRAVITY GRADIENT MEASUREMENTS

Satellite gradiometry offers the potential of determining the global gravity field of the earth with greater detail than alternative satellite schemes. The investigation reported here explores the relative merits of a gradiometer system and a doppler velocity system. The two systems are complementary in that the doppler velocity system is superior for defining the lower harmonic degree variations (less than $\approx 30^{th}$ harmonic degree). The gradiometer system on the other hand gives superior performance for the higher harmonic degrees. The investigation proceeds through four major problem areas:

(1) Determination of a statistical characterization of the sea level gravity anomaly of the earth.

(2) Determination of statistical characterizations of various elements of the gravity field and satellite perturbations at satellite altitude. This statistical characterization is in the form of Power Spectral Density (PSD) curves for the anomalous gravity gradient, gravity anomaly, and finally the radial velocity perturbations of the satellite. The last of these provides a basis for evaluating the doppler velocity system. The procedure followed here is somewhat in contrast with the usual one of using Kaulas rule of thumb to characterize the various anomalies and velocity perturbations at satellite altitude. As will be shown, however, the results are in good agreement particularly at the higher harmonic degrees.

(3) Resolution of instrumentation and associated problems such as satellite attitude, altitude, and position control, optimal orbit determination data handling, etc.

(4) Finally the optimal estimation problem which involves a parameterization of the earth's gravity field and utilization of satellite measurements to establish parameter values.

A discussion of each of these general problem areas is presented to outline the approach, the anticipated problem areas and expected results.

2.1 DETERMINATION OF A STATISTICAL CHARACTERIZATION FOR THE GRAVITY FIELD AT THE EARTH'S SURFACE

A statistical characterization of various gravity related signals (gravity gradient and gravity anomaly, satellite velocity perturbations etc) at satellite attitude is central to an assessment of various satellite based geodetic systems. The usual approach is to use Kaulas' rule of thumb to define these signals. The approach taken here is to use a sea level model for the gravity anomaly and to analytically extend this model to satellite attitudes. Extensive sea level gravity anomaly survey data provides a basis for this approach.

A number of investigations (References 1, 2, 3, 4) have dealt with this problem. The model illustrated by the block diagram on Figure 1 is generally consistent with most of the models developed. A second, shorter correlation distance (D_2) has been introduced so that the sea level gravity gradient anomaly component T_{XZ} ($\frac{\partial^2 T}{\partial_x \partial_z}$) is bounded and in agreement with RMS levels expected.

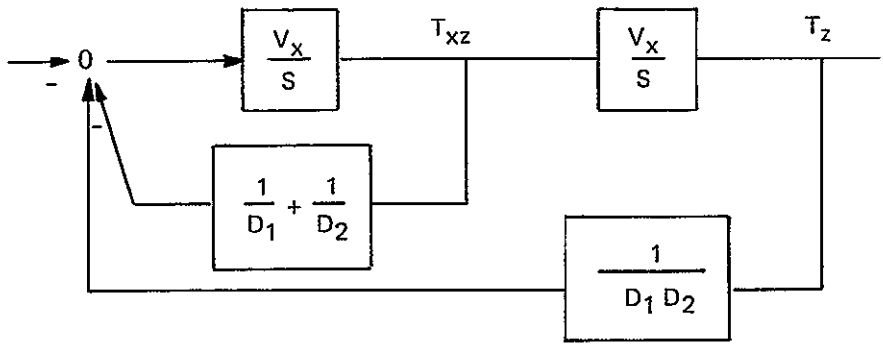

Figure 1. Earth Surface Model of Gravity

where $W = U + T$

W	-	Gravity potential
U	-	Normal component of gravity potential
T	-	Anomalous component of gravity potential
T_i	-	i = x, y, z gravity anomaly components
T_{ij}	-	i, j = x, y, z anomalous components of gravity gradient
D_1, D_2	-	20 nm, 2.5 nm corelation distances
σ_{T_z}	-	40 mgal

2.2 RELATIONSHIP BETWEEN SURFACE ANOMALIES TO MEASURABLE VALUES AT ORBITAL ALTITUDES

At satellite altitudes, the higher spatial frequencies present in the sea level signals will be greatly attenuated. Pizzetti's extension of Stokes integral provides the analytical basis for extending the sea level model to satellite attitude. This integral equation relates gravity potential at satellite altitude to gravity anomaly on the earths surface. The following development details how the gradiometer outputs, which consist of various second spatial derivatives of gravity potential, are related to the sea level anomaly.

A rotating orbital gravity gradiometer in a polar orbit, whose sensitive plane is aligned to the orbit plane, has two outputs . A difference of in line gradients and a cross gradient as follows:

$$E_1(r,\phi,\lambda) = \left(\frac{\partial^2}{\partial r^2} - \frac{1}{r^2}\,\frac{\partial^2}{\partial \phi}\right) T(r,\phi,\lambda) \quad (= T_{ZZ} - T_{XX}) \tag{1}$$

$$E_2(r,\phi,\lambda) = \frac{2}{r}\,\frac{\partial^2}{\partial r \partial \phi}\, T(r,\phi,\lambda) \qquad (= 2T_{XZ}) \tag{2}$$

where ϕ,λ - latitude, longitude

r - orbital radius of an assumed circular orbit

$T(r,\phi,\lambda)$ - anomalous gravity potential at orbital altitude

Pizzetti's extension of Stokes integral relates $T(r,\phi,\lambda)$ to earth surface anomalies;

$$T(r,\phi,\lambda) = \frac{R}{4\pi} \int S(r,\phi,\lambda,\phi',\lambda') \, \delta_g(\phi',\lambda') \cos\phi' \, d\phi' \, d\lambda' \tag{3}$$

where S is Stokes function given by

$$S(r,\phi,\lambda;\phi',\lambda') = \left[\frac{2}{D} + 1 - 3D - t\cos\psi \left(5 + 3\ell n \left(\frac{1-5\cos\psi + D}{2}\right)\right)\right] \tag{4}$$

and $\cos\psi = \sin\phi \sin\phi' + \cos\phi \cos\phi' \cos(\lambda-\lambda')$ (5)

$$\begin{aligned} t &= R/r \\ D &= 1 - 2t\cos\psi + t^2 \\ R &= \text{mean radius of earth} \end{aligned} \tag{6}$$

Substituting 3 in 1 and 2

$$E_1 = \frac{R}{4\pi} \int \left[\frac{\partial^2 S}{\partial r^2} - \frac{\partial^2 S}{r^2 \, \partial\phi^2}\right] \delta_g \cos\phi' \, d\phi' \, d\lambda \tag{7}$$

$$E_2 = \frac{R}{4\pi} \int \left[\frac{2}{r} \frac{\partial^2 S}{\partial r \partial\phi}\right] \delta_g \cos\phi' \, d\phi' \, d\lambda') \tag{8}$$

The bracketed terms in (7) and (8) can be viewed as weighting functions which relate gradiometer outputs to anomaly at ϕ', λ'. Normalized curves for the bracketed terms in equations (7) and (8) are plotted in Figures 2 and 3, respectively. The solid curves in Figure 2 show the weighting function for three satellite altitudes as a function of along track displacement in degrees. The dotted curves show variation with cross track displacement in degrees. The sharper more localized character of the weighting function for low satellite altitudes translates into higher resolution. A spinning orbital gravity gradiometer yields lower resolution cross track than along track. The weighting function shown in Figure 3 $\left(\frac{2\partial^2 S}{r\partial r\partial\phi}\right)$ for the gradiometer output E_2 has odd symmetry with respect to along track displacement. E_2 must approach zero mean over long orbital distances. During a satellite pass over a discrete localized surface anomaly it is evident from the weighting functions that the peak to peak outputs of E_2 and E_1 are the same. Therefore as much information about the earth's gravity field is contained in E_2 as in the signal E_1. Power spectral density plots will show this more explicitly. This result is in contrast to Reeds [7] results which show much lower signal levels for T_{xz} and T_{yz}.

Weighting functions for gradiometer amplitude output E_3 $\left(=\sqrt{E_1^{\,2} + E_2^{\,2}}\right)$ and for T_z $\left(=\frac{\partial T}{\partial r}\right)$ are shown in Figure 4. Both of these are seen to be less localized than E_1 and therefore we should expect lower resolution of the gravity field based on these measurements. Since radial velocity perturbation is dynamically the integral of T_z we conclude that the weighting function for δV is even less localized than that shown for T_z.

The highly localized nature of the weighting functions for E_1 and E_2 permits an approximation in equations (7) and (8) causing them to take on the form of two dimensional convolution integrals. Consequently Fourier transform techniques can be used to characterize these relationships. In particular,

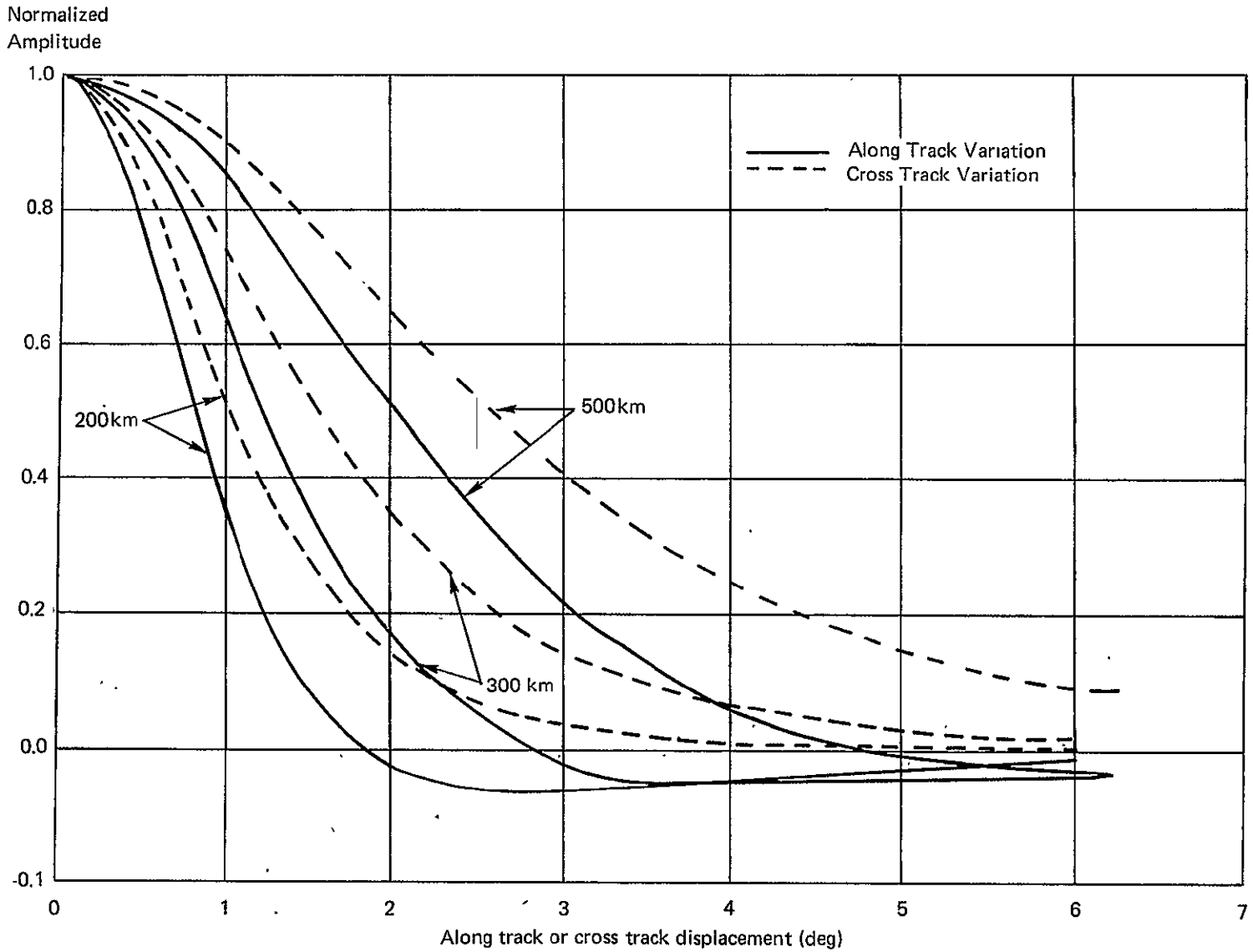

Figure 2. Normalized Weighting Functions for E_1

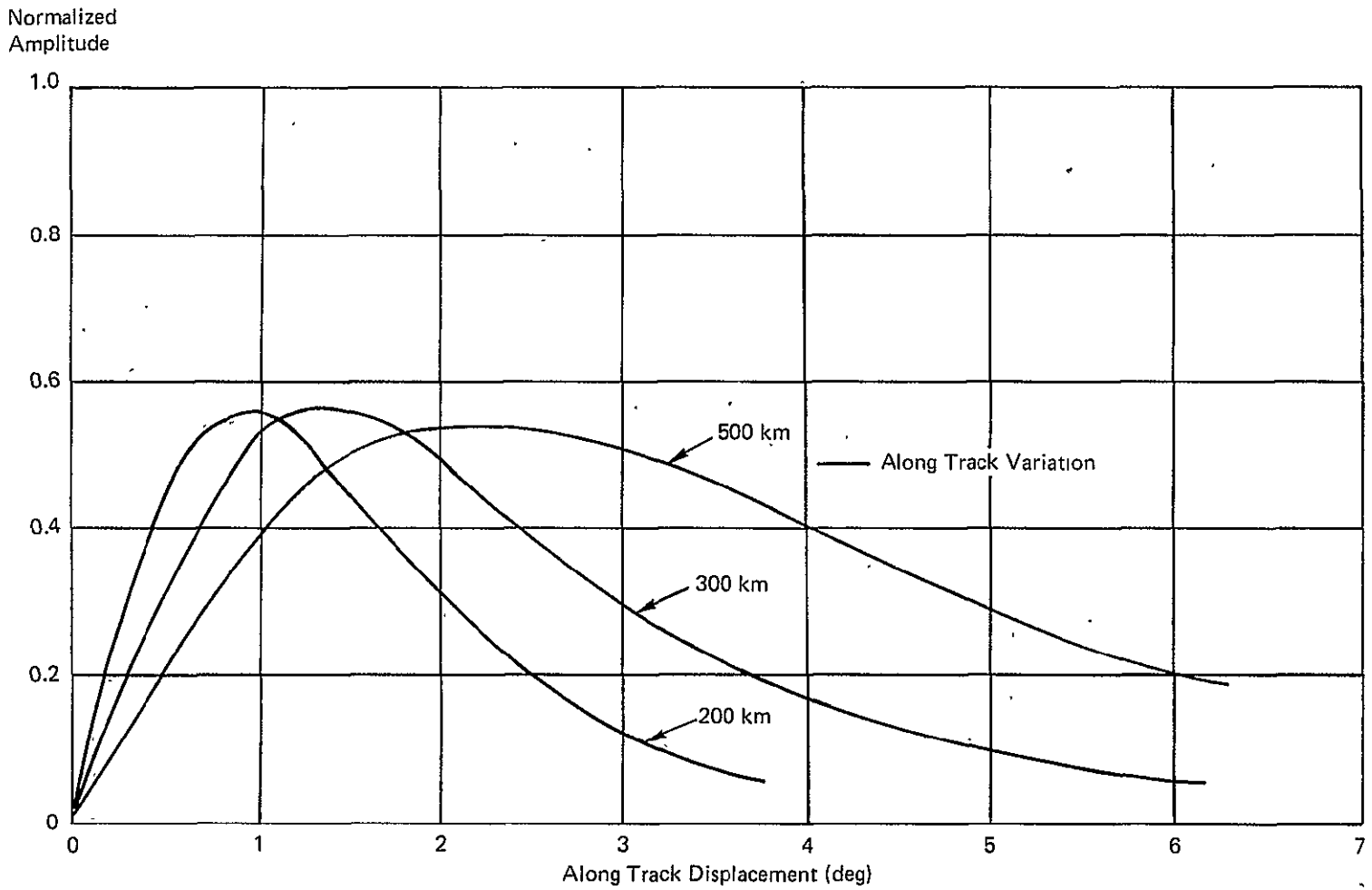

Figure 3. Normalized Weighting Function for E_2

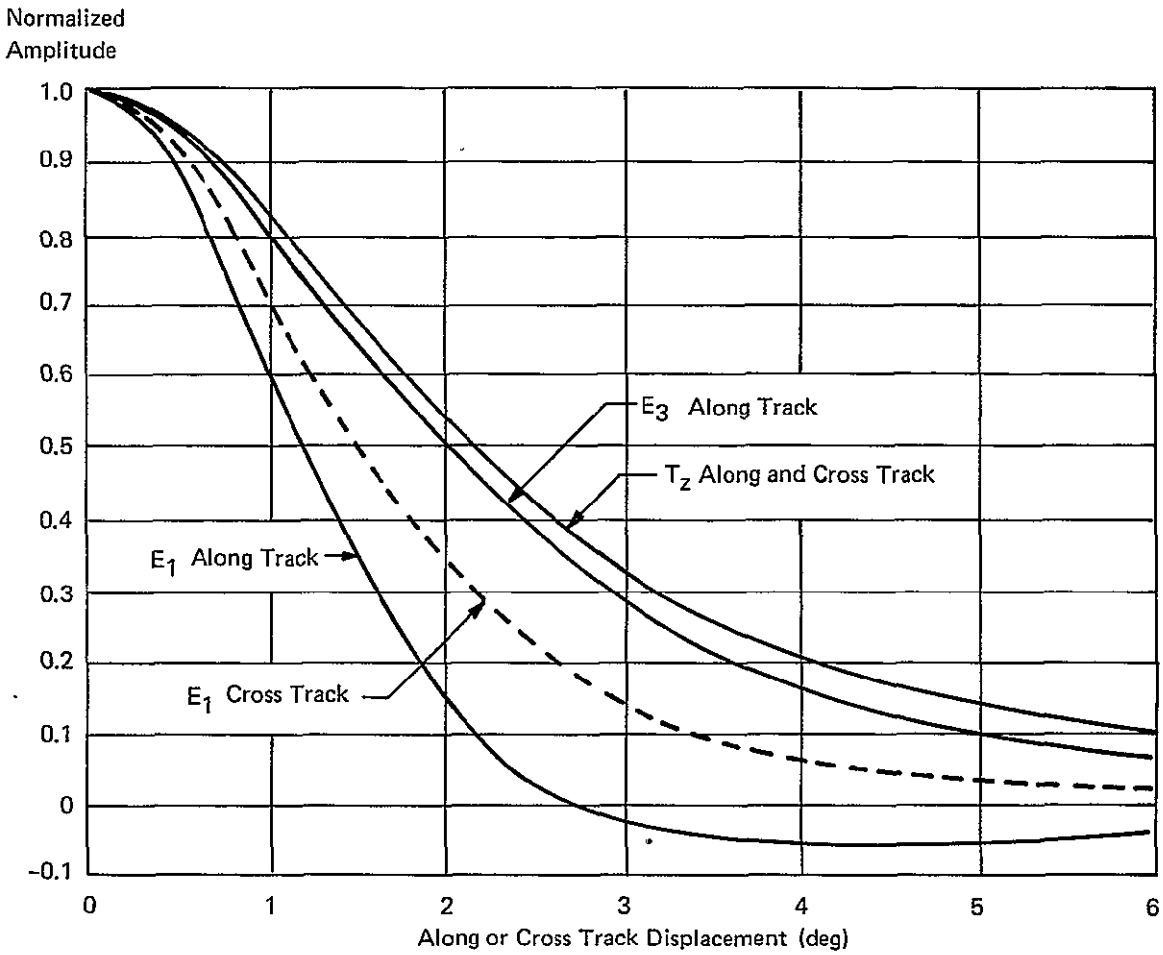

Figure 4. Normalized Weighting Functions for E_1, E_3, T_Z for 300 km Altitude

frequency domain characterization of the signals E_1 and E_2 are possible. To complete the picture all that is required is to relate velocity perturbations of the satellite to these signals. The following matrix differential equation relating anomalous gravity at satellite altitude provides the connection.

$$\begin{pmatrix} \dot{T}_x \\ \dot{T}_y \\ \dot{T}_z \end{pmatrix} = \begin{pmatrix} T_{xx} & T_{xy} & T_{xz} \\ T_{xy} & T_{yy} & T_{yz} \\ T_{xz} & T_{yz} & T_{zz} \end{pmatrix} \begin{pmatrix} V_x \\ 0 \\ 0 \end{pmatrix} = \begin{pmatrix} T_{xx} V_x \\ T_{xy} V_x \\ T_{xz} V_x \end{pmatrix} \qquad (9)$$

In writing equation (9) a circular orbit has been assumed with the x axis directed along track. The dynamics of satellite velocity perturbation is quite complex, however, for the higher harmonic degrees and for error analysis purposes the simple dynamics depicted in Figure 5 is an adequate model of the radial dynamics.

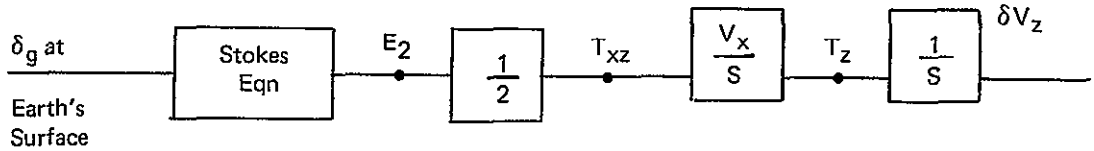

Figure 5. Radial Dynamics Model

This model relates δ_g (earth surface anomalies), the gradiometer output E_2 and radial velocity perturbation δV_Z. A similar model relating E_1 and along track velocity perturbation is not directly possible since E_1 is a measure of T_{XX} in linear combination with T_{yy}.

Using the earth surface model of gravity anomaly and the Fourier transform techniques, the gravity gradient power spectral densities for the signals E_1 and E_2 have been calculated. The power spectral densities for a 300 km orbit are shown in Figure 6. Glaser and Sherry [6] using Kaulus' rule of thumb for T_{ZZ} (equation 10) have approximated the signal E_1 ($= T_{ZZ} - T_{XX}$) by $2T_{ZZ}$.

$$[E_1(n)]^2 \approx [2T_{ZZ}(n)]^2 \approx \left[\frac{GM}{r^3} \times 10^9\right]^2 \left(\frac{R}{r}\right)^{2n} (n+1)(2n+3)^2(2N+1) \times \frac{10^{-10}}{n^4} \tag{10}$$

where n - harmonic degree.

This curve is also plotted in Figure 6 along with Reeds [7] estimate of the gradiometer amplitude output (E_3) which is also based on Kaulas' rule of thumb.

$$E_3^2 = E_1^2 + E_2^2 = (T_{ZZ} - T_{XX})^2 + (2T_{XZ})^2 \tag{11}$$

All of these estimates for gradient signals at orbital altitude are in fairly close agreement particularly at the higher harmonic degrees.

Figures 7, 8 and 9 summarize the PSD's of various signals at three circular orbital altitudes. Table 1 summarizes a set of pertinent values for the three altitudes. Table 2 summarizes the RMS statistics for the signals E_2 and T_2.

Assuming that the gradiometer measurements and the radial velocity doppler measurements are limited by additive white noise, conclusions can be drawn about the required white noise levels and the relative merits of the two instrumentation schemes. Note that white noise of the gradiometer, which has a constant PSD in the E_1^2, E_2^2 plots (Figure 7) varies as $\left(\frac{1}{HD}\right)^2$ on the T_Z^2 plot (Figure 8) and as $\left(\frac{1}{HD}\right)^4$ on the δV^2 plot (Figure 9). By the same token white doppler velocity error (constant PSD on δV^2 plot Figure 9) varies as $(HD)^2$ in the T_Z^2 domain (Figure 8) and as $(HD)^4$ in the E_1^2, E_2^2 domain (Figure 7). Three levels of gradiometer white noise and three levels of doppler velocity white noise are superimposed on the PSD plots of Figure 7. A measure of the resolving power of a particular instrumentation scheme is the harmonic degree at which the instrument white noise level is equal to the signal PSD. Table 3 summarizes the results for the gradiometer while Table 4 does so for the doppler velocity instrumentation. This comparison is based on using the gradiometer output E_2 and the radial velocity perturbation δV_Z. The additional value derived by utilizing E_1 has not been assessed nor has that of instrumenting along track and across track velocity perturbations. Figure 7 shows that for any given white noise levels for the gradiometer and the doppler velocity system there exists a crossover harmonic degree below which the doppler data is of more value than the gradiometer and above which the reverse holds true. Since resolution is a function of the highest harmonic degree of signal power that can be measured, we see that the gradiometer inherently is capable of higher resolution providing the instrument can be built with a sufficiently low white noise level.

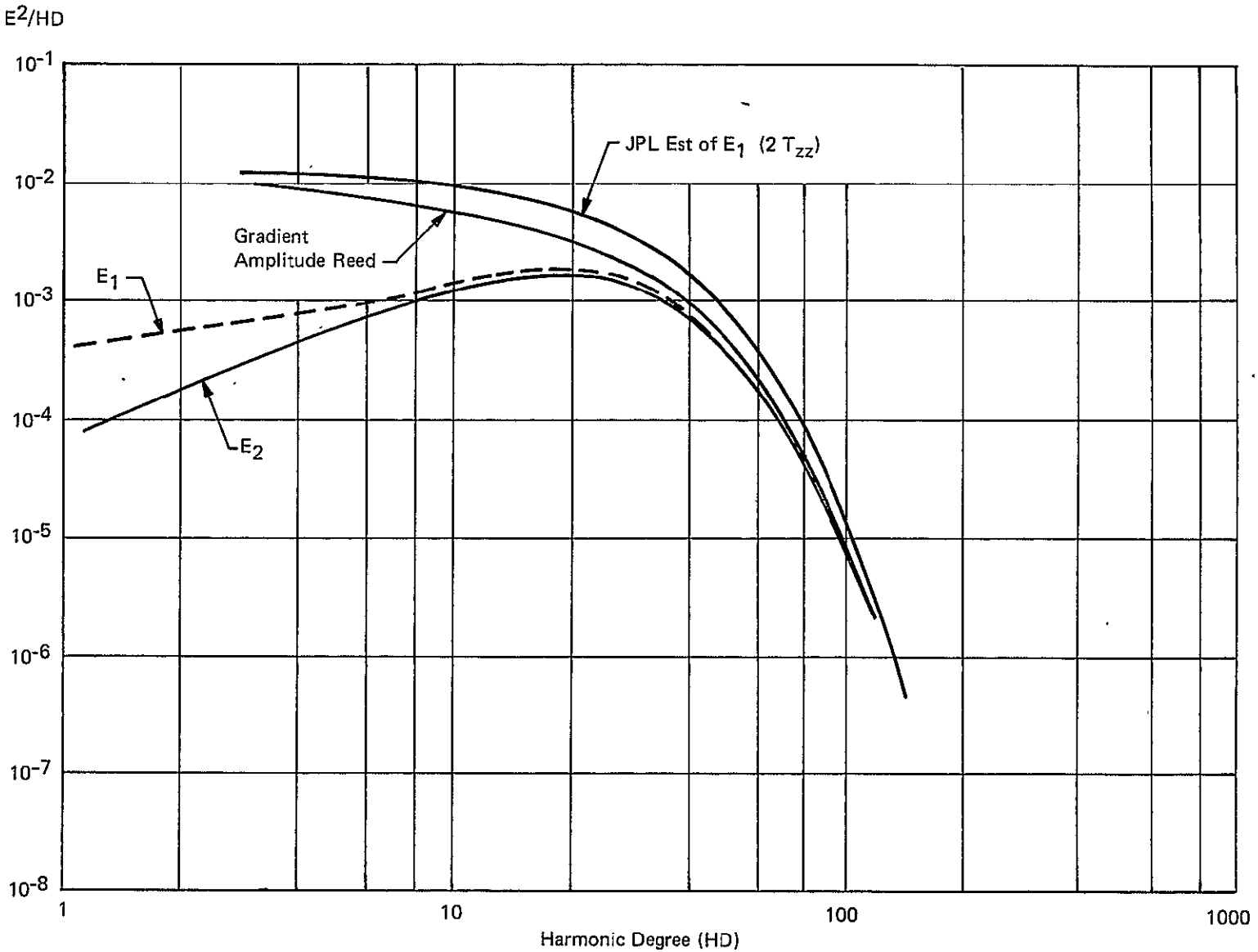

Figure 6. Power Spectral Density at 300 km

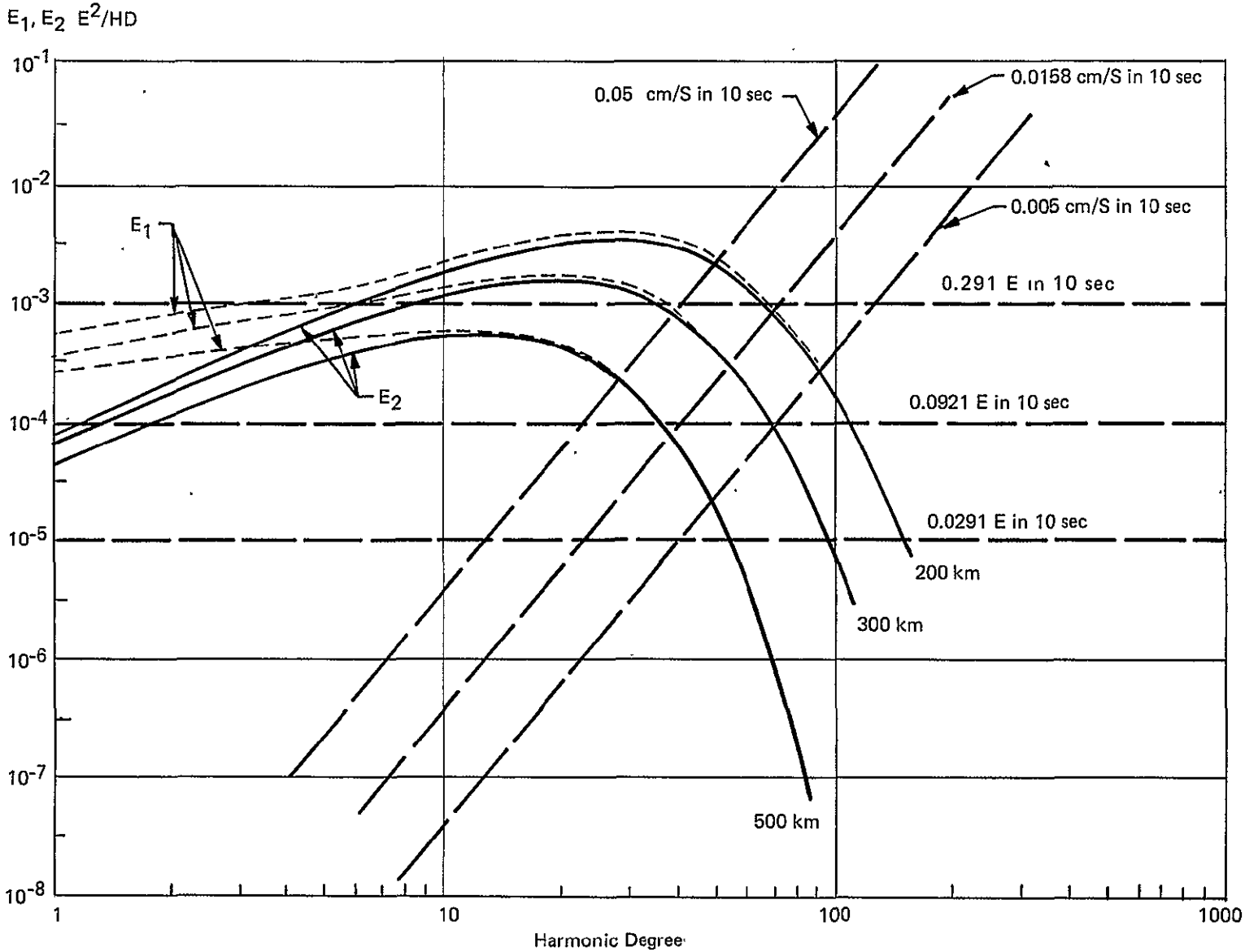

Figure 7. Power Spectral Density Curves for E_1, E_2

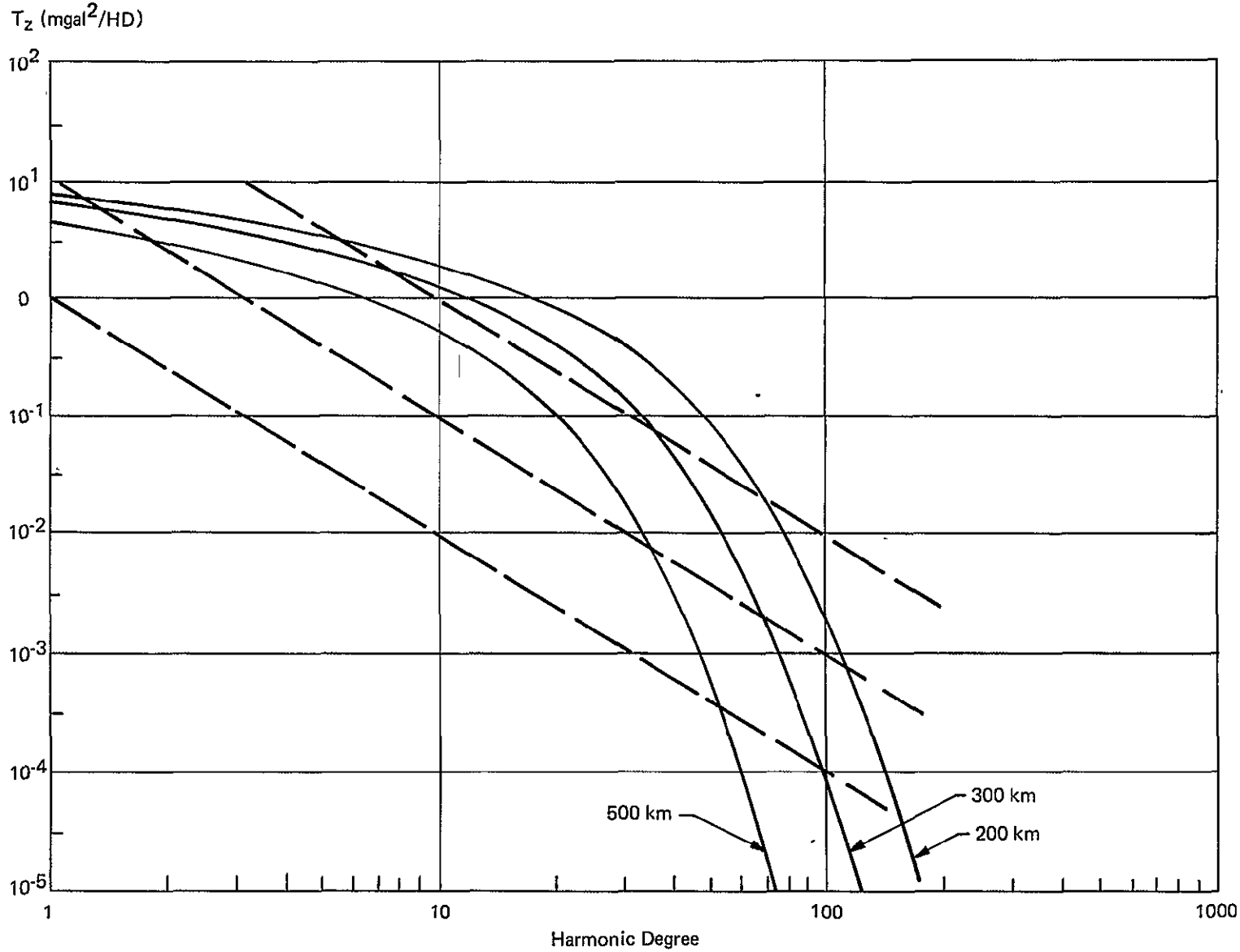

Figure 8. Power Spectral Density Curves for T_z

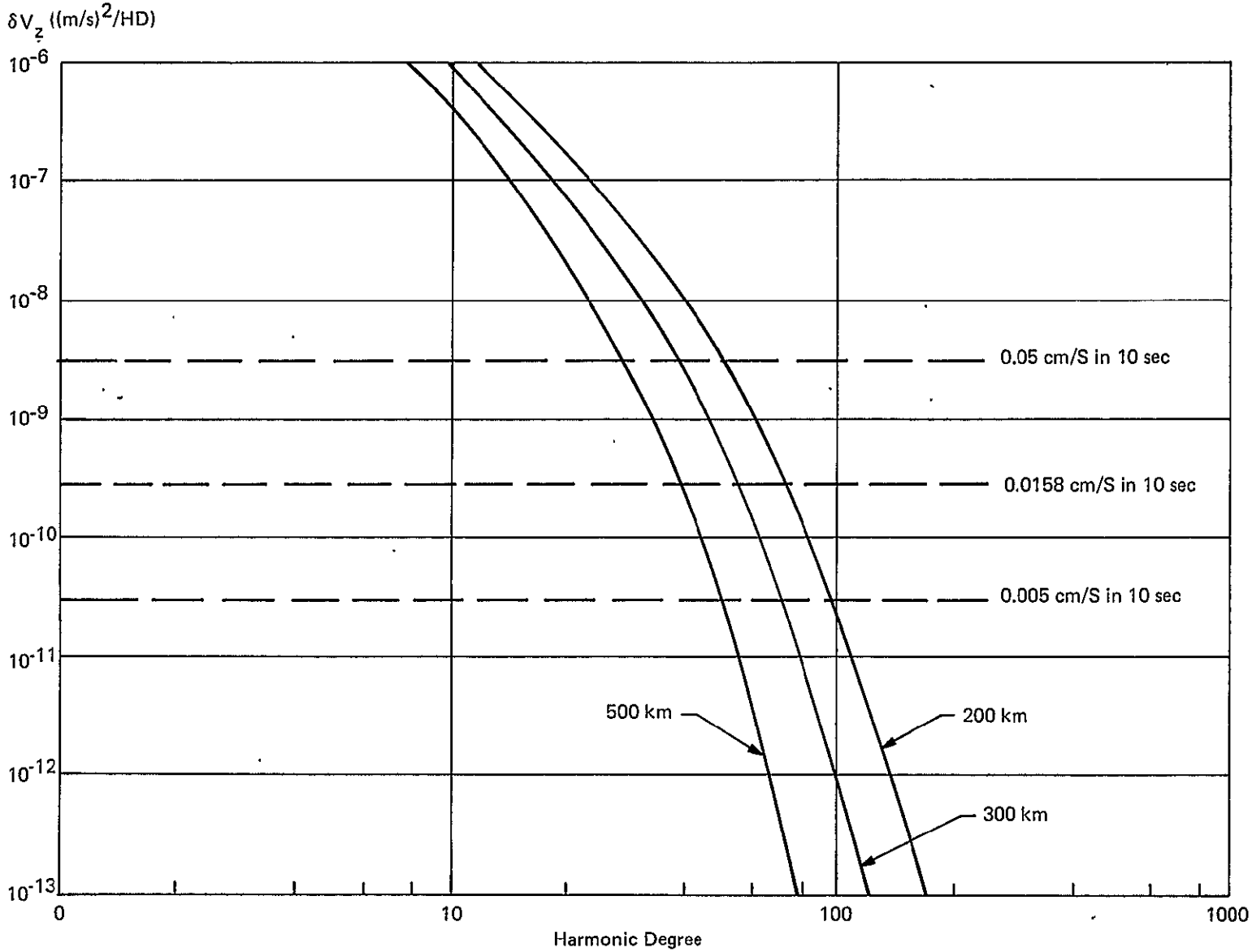

Figure 9. Power Spectral Density Curves for δV_Z

TABLE 1
SATELLITE AND GRADIENT VALUES

Orbit Altitude (km)	$\frac{GM}{r^3}\left(\frac{1}{sec^2}\right)$	ω_o (r/s) $\left(=\sqrt{\frac{GM}{r^3}}\right)$	Orbit Period (Min.)	V (m/s)
0	1.536E-6	0.00124	84.49	7910
200	1.400E-6	0.00118	88.49	7760
300	1.338E-6	0.00116	90.52	7750
500	1.225E-6	0.00111	94.62	7630

GM = 0.398603E15 m^3/sec^2
R = 6.37816E6 m

TABLE 2
RMS VALUES FOR E_2 AND T_z

Orbit Altitude (m)	E^2		T_z	
	$\sigma^2(E^2)$	$\sigma(E)$	$\sigma^2(mgal^2)$	σ (mgal)
200	0.0998	0.315	66.6	8.2
300	0.0360	0.190	48.2	6.9
500	0.00812	0.090	26.9	5.2

TABLE 3
GRADIOMETER INSTRUMENTATION

White Noise Level			Harmonic Degree of Resolution at Orbital Altitude		
E^2/HD	E^2/r/s	E in 10 sec	200 km	300 km	500 km
10^{-3}	0.847	0.291	57	36	--
10^{-4}	0.0847	0.0921	111	67	36
10^{-5}	0.00847	0.0291	150	96	54

TABLE 4
DOPPLER VELOCITY INSTRUMENTATION

White Noise Level			Harmonic Degree of Resolution at Orbital Altitude		
$(M/S)^2$ HD	$(M/S)^2$ r/s	cm/S in 10 sec	200 km	300 km	500 km
2.95×10^{-9}	2.5×10^{-6}	0.05	48	38	28
2.95×10^{-10}	2.5×10^{-7}	0.0158	70	54	38
2.95×10^{-11}	2.5×10^{-8}	0.005	92	69	48

At the 300 km altitude σ_{T_Z} = 6.9 mgal using a 0.03E in 10 sec gradiometer T_Z can be estimated to a level of σT_Z = 0.66 mgal. Using a 0.005 cm/s in 10 sec doppler the result is σ_{T_Z} = 0.12 mgal. If both instruments are used the result is σ_{T_Z} = 0:084 mgal.

2.3 INSTRUMENTATION PROBLEMS

The instrumentation requirements associated with determining satellite position over the earth, its altitude, attitude, etc. for the doppler velocity system differ from those for the gradiometer system. A discussion of some of the salient aspects of these requirements for the two systems follows.

2.3.1 Doppler Velocity System

From a practical point of view, a doppler system involves two or more satellites; one of them being in a relatively low altitude polar orbit, the second being in a higher orbit. The doppler system is instrumented to measure the velocity along the line of sight between the two satellites. Several problems must be resolved.

(1) The velocity perturbation attributable to the low satellite must be determined. The measured signal includes the total velocity difference along the sight line.

(2) The velocity perturbation of the low satellite attributable to gravity anomalies has to be extracted from all sources causing perturbations including solar pressure and orbital drag.

(3) The orbital parameters of the low satellite are varying continuously. This fact presents a problem as to which set of orbital parameters the velocity perturbation is referenced to. This argument applies to the high satellite as well, but its ephemeris changes more slowly.

2.3.2 Gradiometer System

By using a set of four MESA's the gradiometer is capable of discriminating against atmospheric drag, solar pressure forces as well as magnetic torques which may act on the satellite. As a result, the data reduction problem is greatly simplified. The gradiometer mission can be accomplished with a single low altitude polar orbit satellite. A fairly uniform set of measurements covering the globe can be collected in a matter of days.

2.3.2.1 Satellite Altitude Control - If the signal E_1 is to be used, an orbit altitude determination requirement must be imposed. The normal gradient (based on a spherical earth) is given by:

$$U_{ij} = \frac{GM}{r^3} \begin{pmatrix} -1 & 0 & 0 \\ 0 & -1 & 0 \\ 0 & 0 & 2 \end{pmatrix}$$

Variation with altitude is given by

$$\frac{\partial U_{ij}}{\partial r} = \frac{-3GM}{r^4}\begin{pmatrix} -1 & 0 & 0 \\ 0 & -1 & 0 \\ 0 & 0 & 2 \end{pmatrix}$$

at 300 km $\frac{GM}{r^3} = 1338E$ and $\frac{3GM}{r^4} = 7.23 \times 10^{-4}$ E/m

So the normal component of E_1 attributable to radial error is

$$\frac{dE_1}{dr} = 3\left(\frac{3GM}{r^4}\right) = 0.00217 \text{ E/m}$$

If dE_1 is to be held to 0.03E then dr must be known to 13.8 meters.

2.3.2.2 **Attitude Control Requirements** - The major component of the gradient tensor, the normal component, is that due to the earth considered as a point mass. More generally the normal component may represent the gradient due to a low order spherop. The anomalous component used in the data reduction is computed by subtracting from the gradiometer outputs the appropriate normal components. The satellite coordinate system and the computer coordinate system in which the normal component is computed must therefore coincide to some accuracy. The required accuracy of satellite attitude control or determination is analyzed as follows.

The local level orbit coordinate system has its X axis directed along the velocity vector Y axis (satellite spin axis) perpendicular to orbit plane and Z axis vertically downward. The normal gravity gradient in this system is

$$U_{ij} = \frac{GM}{r^3}\begin{pmatrix} -1 & 0 & 0 \\ 0 & -1 & 0 \\ 0 & 0 & 2 \end{pmatrix} = \frac{GM}{r^3}[UN] \tag{12}$$

For the more general case the direction cosine matrix C_N^S relating the normal coordinate system to the satellite coordinate system can be defined in terms of a sequence of angle rotations

$$C_N^S = \begin{pmatrix} \cos\psi & \sin\psi & 0 \\ -\sin\psi & \cos\psi & 0 \\ 0 & 0 & 1 \end{pmatrix}\begin{pmatrix} 1 & 0 & 0 \\ 0 & \cos\phi & \sin\phi \\ 0 & -\sin\phi & \cos\phi \end{pmatrix}\begin{pmatrix} \cos\theta & 0 & -\sin\theta \\ 0 & 1 & 0 \\ \sin\theta & 0 & \cos\theta \end{pmatrix} \tag{13}$$

A small angle deviation from this nominal orientation can be treated as a vector.

$$\Delta C_N^S \begin{pmatrix} 1 & \delta\psi & -\delta\theta \\ -\delta\psi & 1 & \delta\phi \\ \delta\theta & -\delta\phi & 1 \end{pmatrix} = \begin{pmatrix} 1 & 0 & 0 \\ 0 & 1 & 0 \\ 0 & 0 & 1 \end{pmatrix} + \begin{pmatrix} 0 & \delta\psi & -\delta\theta \\ -\delta\psi & 0 & \delta\phi \\ \delta\theta & -\delta\phi & 0 \end{pmatrix} =$$

$$= I + [\delta A] \tag{14}$$

The error in gravity gradient ΔT_{ij} due to the attitude uncertainty ΔC_N^S is given by;

$$\Delta T_{ij} = \frac{GM}{r^3} \left| (I + [\Delta A])\, C_N^S\, [UN]\, (C_N^S)^T\, (I + [\delta A])^T - C_N^S\, [UN]\, (C_N^S)^T \right| \tag{15}$$

$$\Delta T_{ij} = \frac{GM}{r^3} \left| C_N^S\, [UN]\, (C_N^S)^T\, [\delta A]^T + [\delta A]\, C_N^S\, [UN]\, (C_N^S)^T \right.$$

$$\left. + [\delta A]\, C_N^S\, [UN]\, (C_N^S)^T\, [\delta A]^T \right| \tag{16}$$

For the special case where the satellite is controlled to the nominal attitude $C_N^S = I$ and equation 16 becomes

$$\Delta T_{ij} = \frac{GM}{r^3} \left| [UN]\, [\delta A]^T + [\delta A]\, [UN] + [\delta A]\, [UN]\, [\delta A]^T \right| \tag{17}$$

Evaluating this expression, the result to first order off diagonal and 2nd order diagonal is;

$$\Delta T_{ij} \frac{GM}{r^3} \begin{pmatrix} -\delta\psi^2 + 2\delta\theta^2 & 0 & -3\delta\theta \\ 0 & -\delta\psi^2 + 2\delta\phi^2 & 3\delta\phi \\ -3\delta\theta & 3\delta\phi & -\delta\theta^2 - \delta\phi^2 \end{pmatrix} \tag{18}$$

The corresponding error in the two gradiometer outputs are therefore;

$$\Delta E_1 = \frac{GM}{r^3} \left[-\delta\theta^2 - \delta\phi^2 - (-\delta\psi^2 + 2\delta\theta^2) \right] = \frac{GM}{r^3} \left[-3\delta\theta^2 - \delta\phi^2 + \delta\psi^2 \right] \tag{19}$$

$$\Delta E_2 = \frac{GM}{r^3} 2\,[-3\delta\theta] = -\frac{GM}{r^3} 6\delta\theta \tag{20}$$

Equation 20 implies $\Delta T_{XZ} = -\frac{GM}{r^3} 3\delta\theta$

As described elsewhere in this report the signal E_2 can be used on a long term average basis to define the pitch attitude of the satellite. As a result $\delta\theta$ can be controlled or known to negligibly low level. If the error in E_1 is to be controlled to less than 0.03 E for example, equation (19) requires,

$$\delta\psi^2 - \delta\phi^2 \leqslant \frac{0.03}{GM/r^3} = \frac{0.03}{1338} = 2.24 \times 10^{-5}\ \text{rad}^2 \tag{21}$$

for the 300 km orbit. If we neglect the higher harmonic degree attitude perturbations the satellite axis tends to remain stationary in inertial space, hence roll and yaw errors vary at orbit rate as follows:

$$\delta\psi = \delta_0 \sin(\omega_0 t + \gamma)$$

$$\delta\phi = \delta_0 \cos(\omega_0 t + \gamma)$$

where δ_0 is the total angular deviation of the satellite axis relative to the orbit plane direction,

ω_0 - orbital rate

γ - defines the direction of the angular deviation δ_0

Evaluating 21 the result is:

$$\delta\psi^2 - \delta\phi^2 = -\delta_0^2 \cos(2\omega_0 t)$$

If we require the peak error $\leqslant 0.03E$ then $\delta_0 \leqslant 0.271°$.

With respect to determining position, altitude, attitude, etc. the potential of accomplishing real time space navigation merits investigation. A satellite equipped with a gradiometer made up of sensitive accelerometers such as the MESA, has the basic elements necessary to implement real time space navigation. The low polar orbit satellite will experience significant drag and gravity anomaly forces which can be sensed by the MESA's and the gradiometer. Real time ephemeris updating should be possible using this data. The gradiometer data is also useful in establishing a coordinate system by virture of defining the local vertical. Real time orbital parameter computation could lead to significant relaxation of ground tracking requirements.

2.4 DETERMINATION OF THE EARTH'S GRAVITY FIELD BASED ON MEASUREMENTS MADE IN ORBIT

At the outset, it would appear that a spherical harmonic parameterization of the earth's gravity field would be the most natural. Several investigators [5, 7], however, have used an alternative parameterization which divides the earth's surface into lattitude, longitude squares. The optimal estimation problem involves determination of the mean anomaly for each of these areas. This alternative parameterization is made possible by the highly localized nature of the gravity gradient weighting functions. Argentiero and Garza-Robles [5] demonstrate near orthogonality of a core of squares imbedded in a larger block of gradiometer data. The spherical harmonic parameterization by contrast does not permit localized solutions based on localized data.

The long term average output of the gradiometer signal E_2 ($= 2T_{XZ}$) must statistically approach zero. The output E_2 ($= W_{ZZ} - W_{XX}$) on the other hand includes a normal component of $\frac{3GM}{r^3}$ ($\approx 4014E$ at 300 km). Consequently E_1 or E_3 (Gradient amplitude) measurements to an accuracy of 0.03E require scale factor stability of 7.5×10^{-6} ($= \frac{0.03}{4014}$). Scale factor stability to this level may be difficult to achieve. The implications of this as it relates to the data reduction problem are pervasive. A geographically localized block of data in general spans several days in time. If the signals E_1 or E_3 are to be used in the data reduction it will be necessary to model and estimate or control long term variations in scale factor. The net result is that cross track resolution will be further degraded over that of the basic instrument. The long term stability problems might be controlled by utilizing the high redundancy of data taken over the polar regions. Short term signal variations (10th to 100th harmonic degree) occurring during a single pass will be much less corrupted by scale-factor variations. The signal E_2 being a zero mean signal is virtually unaffected by scale factor stability.

A detailed analysis of the data reduction problem utilizing the signals E_1 and E_2 and modeling long term scale factor stability should be carried out to resolve these problems. Such an analysis would also answer quantitatively the questions of cross track resolution and along track resolution for estimating the earth's gravity field.

2.5 REFERENCES

1. Shaw, L; Paul, I; and Henderson, P; Journal of Geophysics Research, Vol. 74, No. 17, Aug. 15, 1969.

2. Jordan, Stanley K., IEEE Transactions on Aerospace and Electronic Systems, Vol. AES-9, No. 5, Sept. 1973.

3. Kasper, Jr., J.F., "A Second-Order Markov Gravity Anomaly Model," Journal of Geophysical Research, Vol. 76, No. 32, November 1971, pp. 7844-7849.

4. Metzger, E.H., Jircitano, A., "Analysis of Real Time Mapping of Horizontal and Vertical Gravity, Anomalies Aboard a Moving Vehicle Such As An Aircraft," International Symposium on Applications of Marine Geodesy, June 3-5, 1974, Columbus, Ohio.

5. Argentiero, P; Garza-Robles, R., "Simulation of a Lunar Gradiometer Mission" NASA X-932-74-358, preprint, December 1974.

6. Glaser, R. and E.J. Sherry (1972) Comparison of Satellite Gravitational Techniques, Jet Propulsion Laboratory, C.I.T., Pasadena.

7. Reed, George B., "Application of Kinematical Geodesy for Determining the Short Wavelength Components of the Gravity Field by Satellite Gradiometry," The Ohio State University Research Foundation, Report No. 201, March 1973.

3.0 ROTATING ACCELEROMETER GRAVITY GRADIOMETER CONCEPT

The previous section outlined the merit of global gravity mapping using an orbital gravity gradiometer. Gravity anomalies could be mapped to much higher harmonic degrees and in a shorter period of time than possible with present techniques. The question therefore is whether an orbital gravity gradiometer is feasible within the present state of the art of instrumentation, at a realistic cost and with sufficiently high confidence level of success to warrant a satellite mission for this purpose.

Bell has been under contract to SAMSO USAF to develop a feasibility model of a rotating accelerometer gravity gradiometer for airborne application since April of 1974. It is the objective of that program to solve the very difficult instrumentation problem of moving base gravity gradiometry within the present state of the art and application of proven and qualified instruments. Sufficient progress has been made to demonstrate gravity gradient measurements in the laboratory to 1 EU in a ten second time period with excellent operational characteristics.

3.1 DESCRIPTION OF ROTATING ACCELEROMETER GRAVITY GRADIOMETER CONCEPT

Dynamic gravity gradiometry constitutes an extremely difficult instrumentation problem. 0.03 EU gravity gradient corresponds to an acceleration difference of 3×10^{-12} g at two points 1 meter apart which has to be measured in the presence of vehicle disturbances. On the earth this will include vehicle acceleration in addition to the full 1 g gravity vector. In orbit the maximum acceleration levels experienced will be under 10^{-5} g. This much lower acceleration environment in space is the major reason that gravity gradient measurements to 0.03 EU are deemed feasible aboard an orbital vehicle.

At first glance measuring acceleration differences to 10^{-12} g at two points 1 meter apart appears to pose an unsurmountable instrumentation problem.

The null bias, the output in the absence of an input, of a good force rebalance accelerometer, such as the Bell Model VII, is in the order of 20 micro g with a randomness of a few tenths of microg's as illustrated on Figure 10. At first glance extracting acceleration inputs 5 order of magnitudes smaller than the null bias noise does not appear feasible. A power spectral analysis of a typical null bias run of many hours is shown in Figure 11. The power spectral density of the null bias is high at the low frequencies but falls off to very low level at frequencies above a revolution per minute.

Null bias is produced by non-acceleration induced forces on the proof mass of the accelerometer. Figure 12 shows a cut-away section of the Model VII accelerometer which is used with the airborne gravity gradiometer, to illustrate the nature of null bias and also to highlight the benefits obtained by using the Miniature Electrostatic Accelerometer for the orbital gravity gradiometer. The cylindrical proofmass is shown suspended by flexure springs. The proof mass has a tendency to hang back with acceleration along the sensitive or input axis. This deflection is sensed by a capacitive pick-off. An electronic loop operating from this pick-off signal generates a current which is injected into a coil mounted inside the proof mass. This current interacts with a strong magnetic field produced by the conical Alnico V magnets to restore the proof mass to the null position. The force rebalance current is the output signal of the accelerometer.

Should a plate of the capacitance pick off system be slightly displaced or should the zero torque position of the suspension spring change slightly because of a change in temperature or aging characteristics of materials, a current would be required to maintain the proof mass in the pick off null position. For these reasons all inertial instruments are to some extent thermometers and indicators of aging characteristics of materials and hence the slow variation in null bias with time and high bias power spectral densities at very low frequencies.

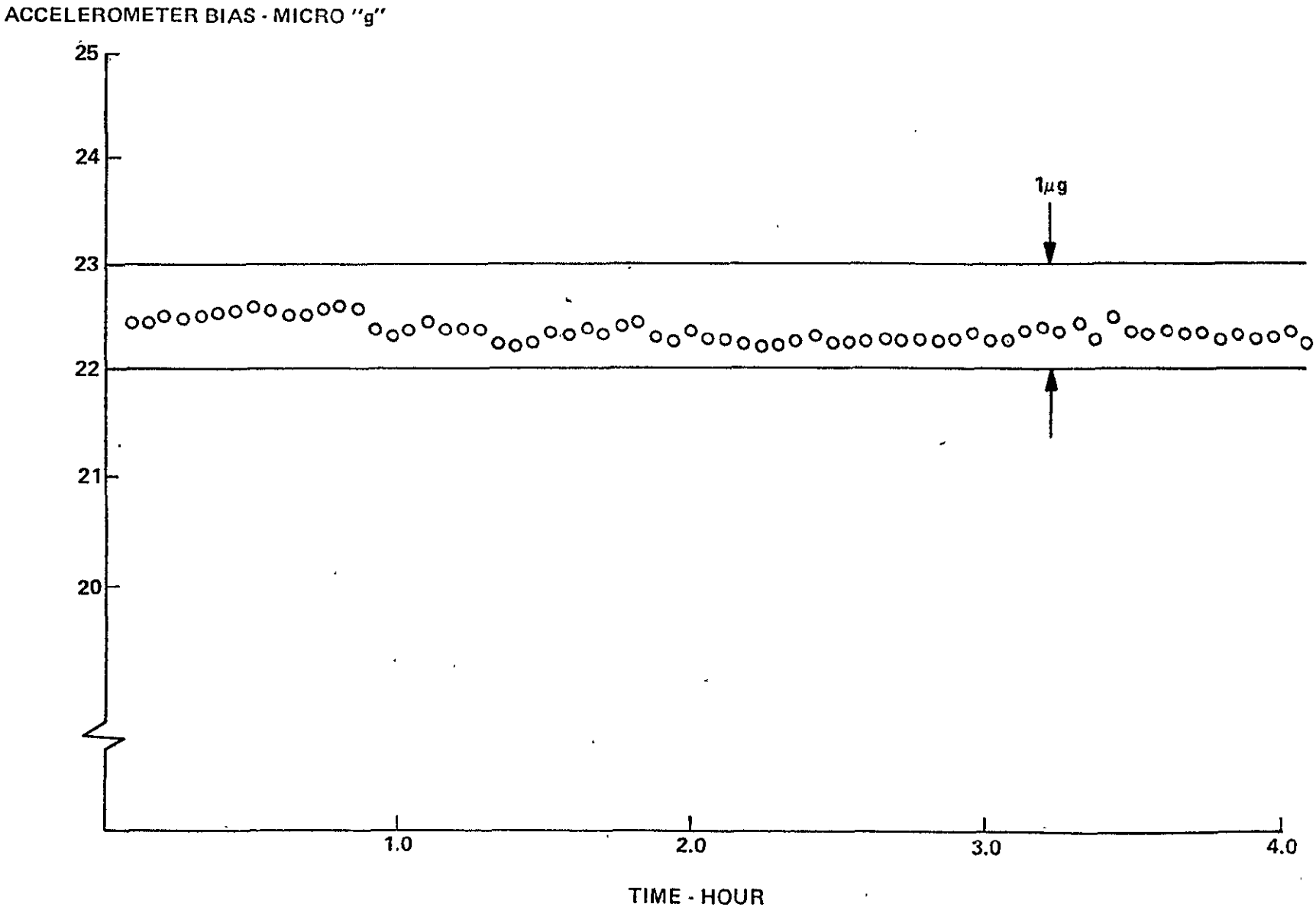

Figure 10. Typical Accelerometer Null Bias

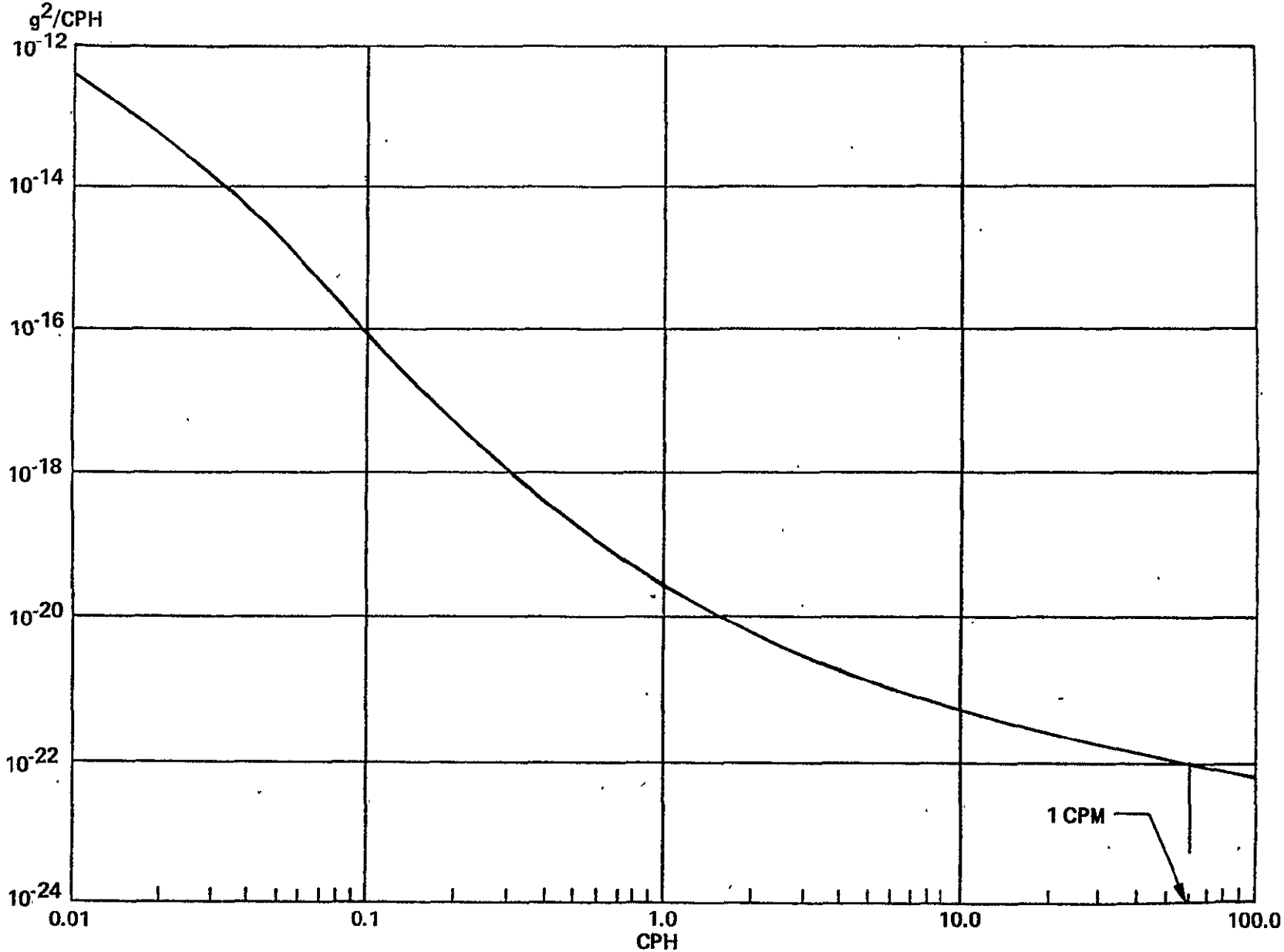

Figure 11. Typical Accelerometer Null Bias Power Spectrum

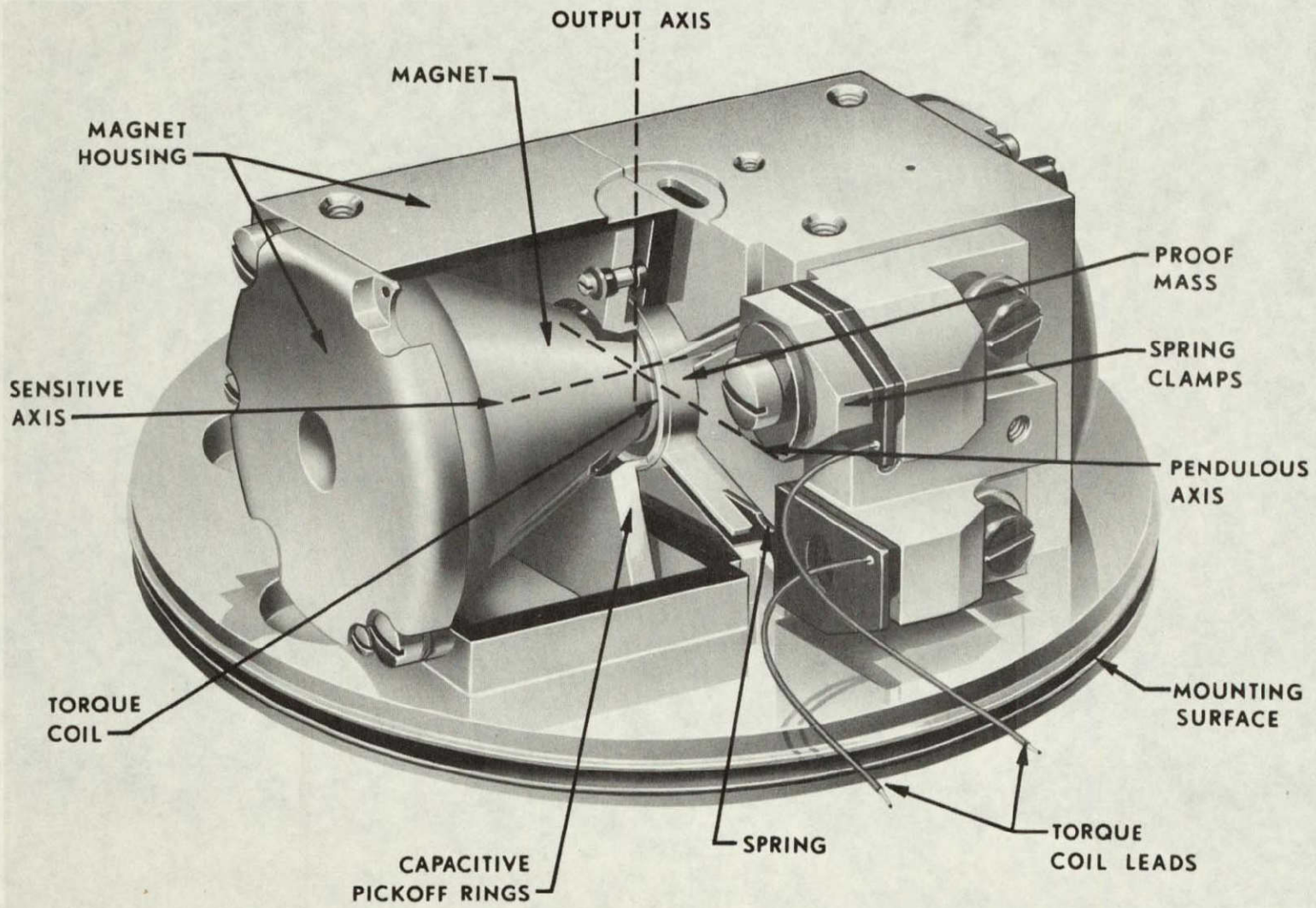

Figure 12. Model VII Accelerometer

The MESA with its scalable electrostatic suspension system exhibits much better null bias characteristics than accelerometers with conventional flexure suspension systems. This is discussed in the next section of this report.

If the gravity gradient information could be shifted to a higher frequency region in the order of a revolution per minute or more, detection of the minute gravity gradient signals would clearly become possible as indicated by the power spectrum in Figure 11. This is accomplished by mounting four accelerometers on a rotating fixture as illustrated schematically by the diagram of Figure 13. Each accelerometer will still exhibit its own null bias in the very low frequency domain.

The input linear acceleration experienced by each accelerometer will be modulated at the rotation speed Ω, and the gravity gradient signal will be modulated at twice rotation frequency 2Ω. The gravity gradient signal has been separated in the frequency domain from the unwanted noise by Ω and 2Ω, and the information can be extracted by synchronous demodulation. In addition, unwanted signals are cancelled by common mode rejection made possible by proper summation of the four accelerometers. The output of opposing pair of accelerometers $(a_1 + a_2)$ and $(a_3 + a_4)$ are summed to reject the linear acceleration within the scale factor balance of the two instruments for two reasons. Since the fixture is rotated relatively slowly it would require a very long filtering time to separate the large output at 1Ω caused by linear accelerations from the very small gravity gradient output at twice rotation speed 2Ω. Furthermore, linear acceleration inputs at or near the rotation frequency would produce an error signal at twice rotation frequency.

A spinning orbital vehicle will experience some linear acceleration inputs at twice rotation speed because of orbital drag being modulated by imperfections in the geometry of vehicle. A second pair of accelerometers is mounted to the fixture in space quadrature and their summed output subtracted from the first to minimize the effect of angular modulation at twice spin speed which would be fully measured by only one pair. An additional benefit of the four accelerometer is the multiplication of the gravity gradient output by a factor of two.

The rotating accelerometer gravity gradiometer is inherently a two axis device, measuring the difference of in-line gradients on one channel and the cross gradient on the other. For example, a rotating accelerometer gradiometer with a horizontal rotation axis moving along the north (x) axis is illustrated schematically by the gradiometer in the background of Figure 13, and this will be the orientation of the satellite gradiometer in a polar orbit except of course at much higher altitudes.

3.2 ACCELEROMETER SCALE FACTOR BALANCE LOOPS

As pointed out, pairs of accelerometers are used with the rotating accelerometer gravity gradiometer to reject linear accelerations within the scale factor balance of accelerometers in each pair. If the scale factors of the accelerometers in each pair were exactly equal, linear acceleration inputs would be totally cancelled because the input axis of the accelerometers in each pair are pointing in opposite directions. Long experience with inertial instruments has shown that balances between two accelerometers to 10^{-4} are relatively easy to achieve and maintain. Balances of 10^{-6} or better are not only very difficult to attain but cannot be maintained very long because of material and electronic component instabilities. To tolerate a reasonable acceleration environment at the spin frequency, scale factor balances of 10^{-9} are desirable.

However, the system is continuously informing us as to the state of the scale factor balances of the two accelerometers in each pair by an output signal at the rotation frequency in conjunction with a steady state acceleration input. On the earth the steady state acceleration is provided by gravity and in orbit by

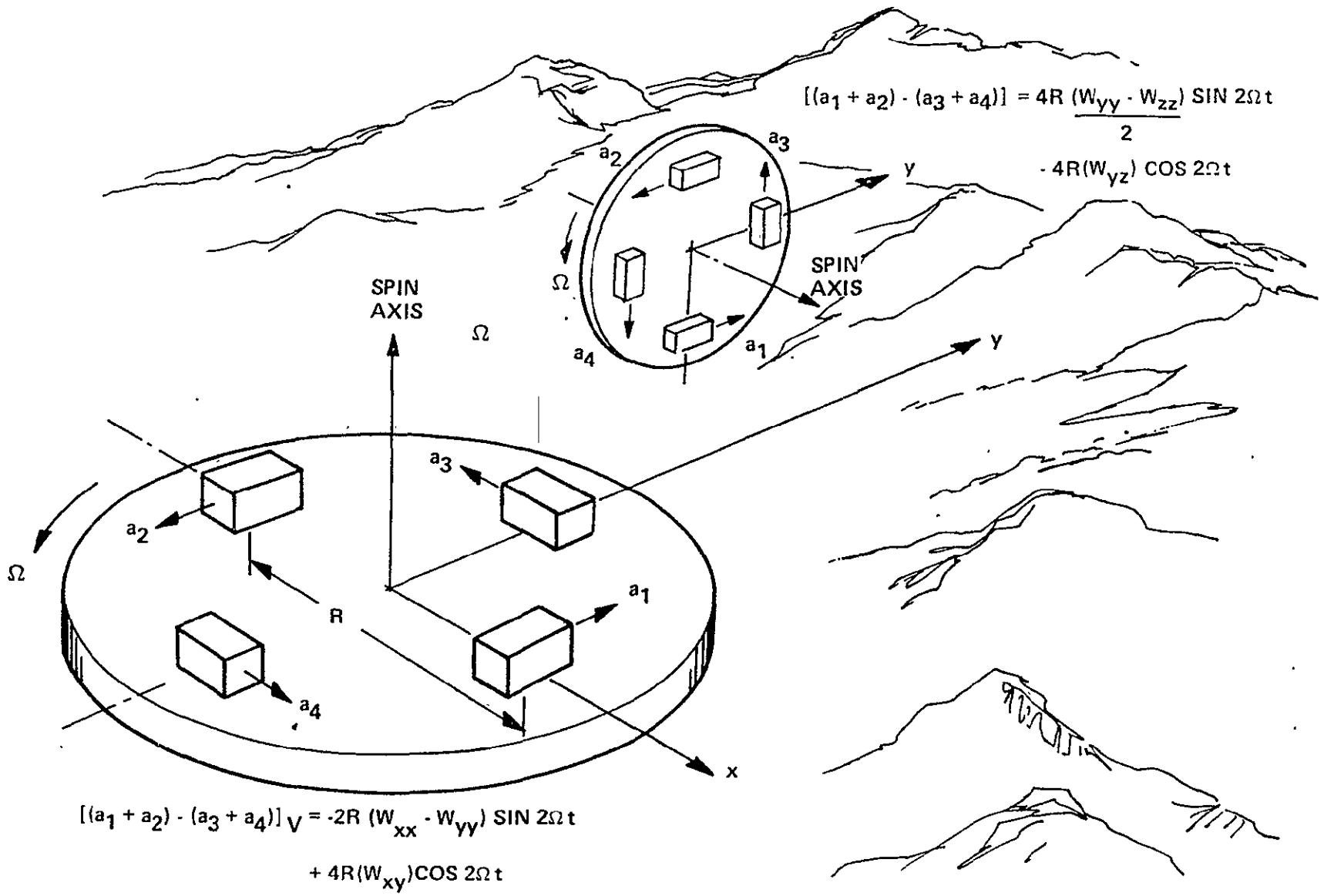

Figure 13. Schematic of Rotating Fixture in Shake Structure

orbital drag. The output of the gradiometer is demodulated by the sin and cos of the spin speed (Ω) and the resultant signal integrated and applied to adjust the scale factor of one accelerometer in each pair until the signal at the rotation frequency disappears.

Block diagram Figure 14 illustrates the scale factor balance loops. Theoretically a very high degree of scale factor balance is achievable because relatively long time constant loops are permissible since scale factors change only slowly. With the Model VII accelerometer the scale factor balances are adjusted by injecting a current into coils wound around the Alnico magnets. The MESA scale factors are adjusted by controlling the dc forcer voltage. These scale factor balance loops have been implemented and are operating well.

The second scale factor balance loop adjust the summed scale factor balances of accelerometers $a_1 + a_2 = a_2 + a_3$ to reject angular modulation of the spin speed at twice rotation speed. A considerable amount of twice speed angular modulation has to be expected from the rotating mechanism, bearings, torque motor, tachometer and slip rings of the airborne gravity gradiometer. The rotating fixture is oscillated through a small angle at a frequency non-synchronously related to the spin speed. The signal demodulated at this frequence is a measure of the scale factor unbalance of the summed pairs. The scale factor of an additional accelerometer is adjusted until a balance is obtained as illustrated by block diagram, Figure 15.

Whether these scale factor balance loops will be required for the orbital gravity gradiometer depends on the amount of linear acceleration at the spin speed and twice spin speed angular modulation experienced aboard the spinning vehicle. Mechanisms for both type of distrubances are known and should their magnitude require it, these balance loops can be easily incorporated in the orbital gravity gradiometer.

The status of the airborne gravity gradiometer development program is presented in Section 5.0 of this report and the results form the foundation for the orbital gravity gradiometer.

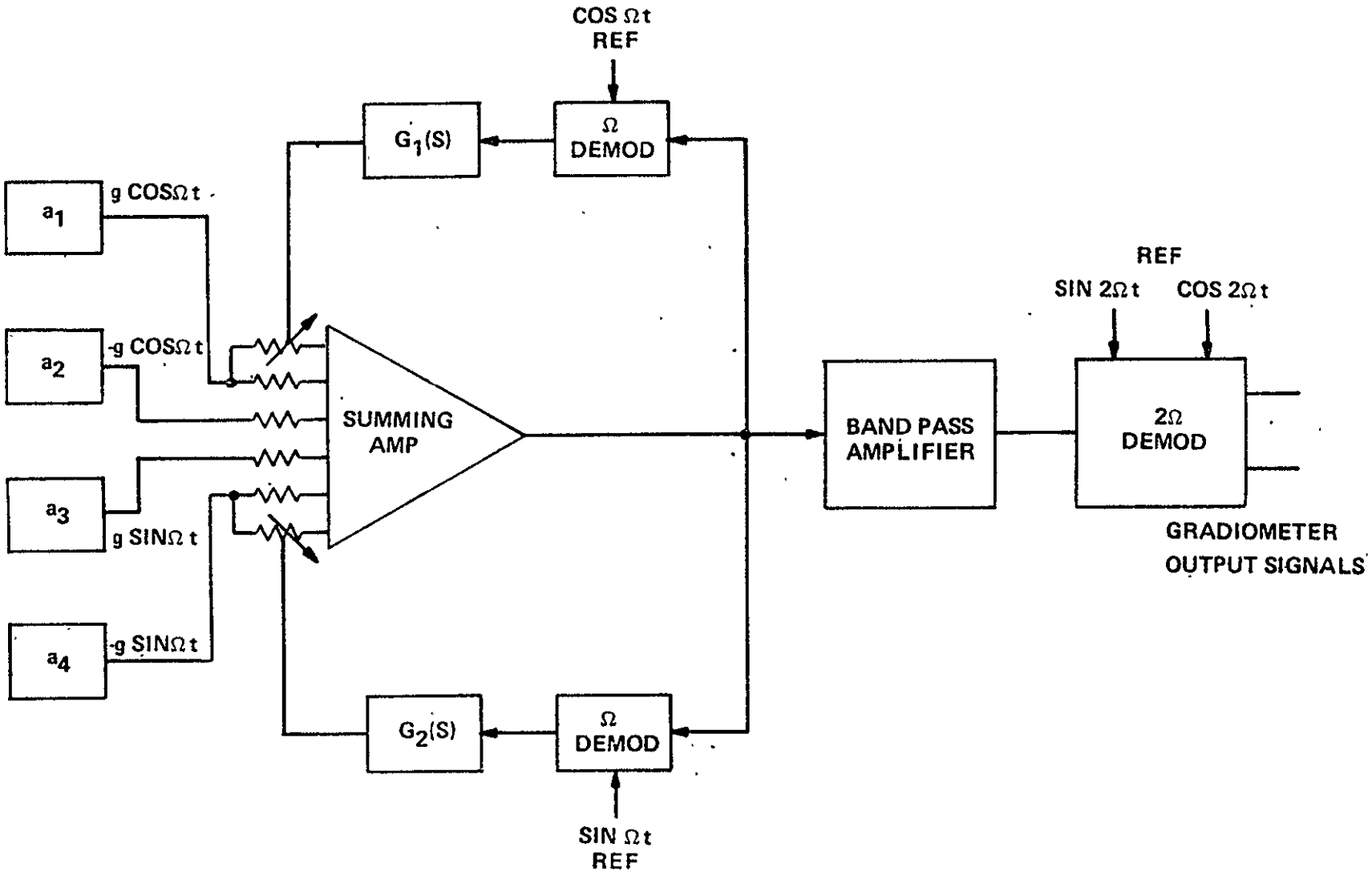

Figure 14. Automatic Scale Factor Balance Loop No. 1

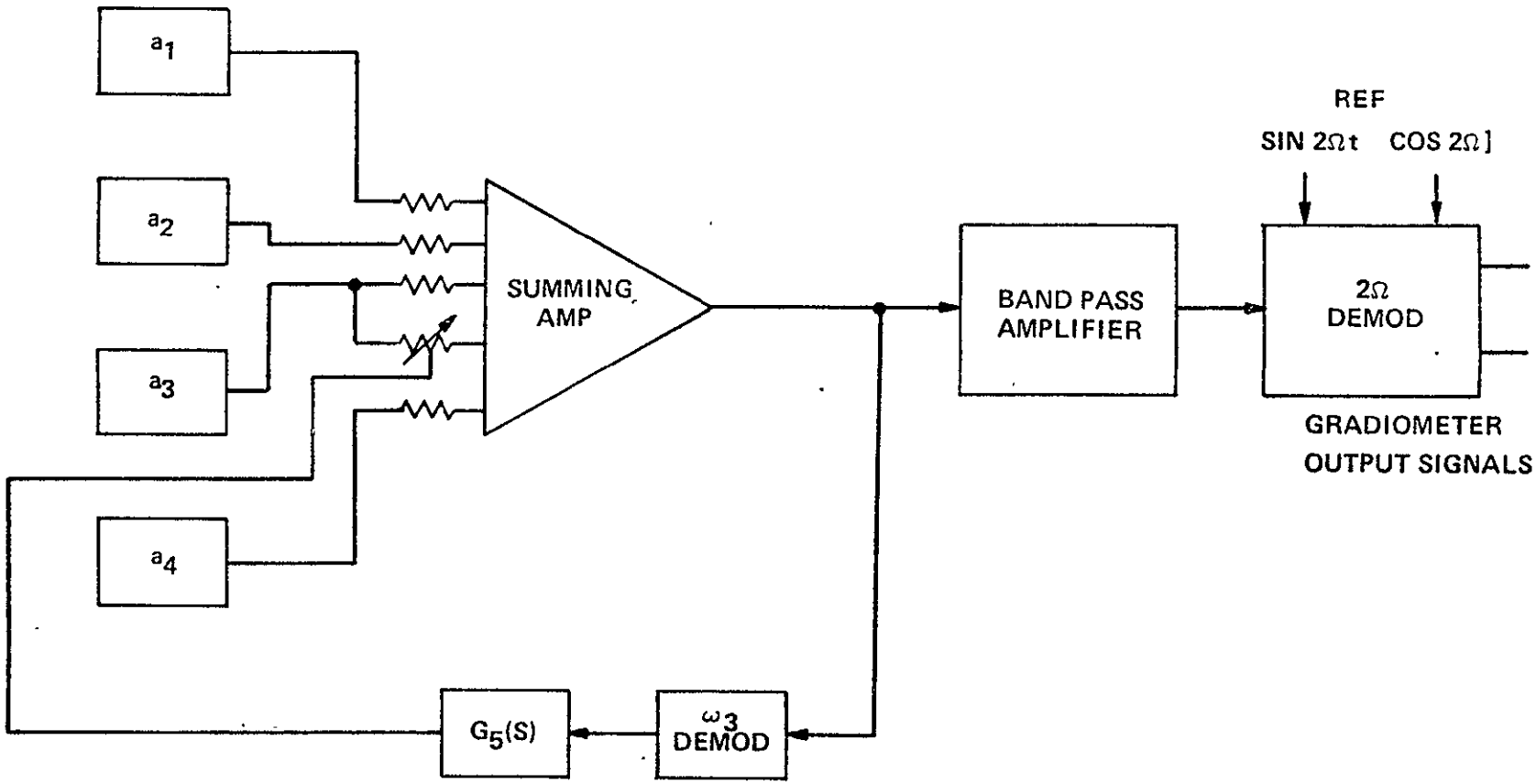

Figure 15. Automatic Scale Factor Balance Loop No. 2

4.0 ORBITAL VERSION OF ROTATING ACCELEROMETER GRAVITY GRADIOMETER

The orbital version of the rotating accelerometer gravity gradiometer is discussed in this section. Miniature Electrostatic Accelerometers (MESA) are substituted for the Model VII used for the airborne gravity gradiometer and the spinning orbital vehicle serves as the rotating platform. The MESA's potentially generate less noise to permit gravity gradient measurements to 0.03 EU in a ten second time period. The slowly spinning orbital vehicle (0.2 rad/sec) potentially provides an almost perfect rotating fixture as contrasted with the bearing supported, torque motor driven device which is presently used and hence will eliminate many of the noise sources introduced by these components.

The analysis covers the performance to be expected from a slowly spinning orbital gravity gradiometer using four MESA's. Two general areas of error mechanism are discussed, self generated noise from the MESA instruments and noise introduced by the rotating satellite. Critical requirements for the spacecraft are outlined to allow gravity gradient measurements to 0.03 EU.

4.1 MINIATURE ELECTROSTATIC ACCELEROMETER (FIGURE 16)

The Bell MESA is of the force feedback type specifically designed for low level acceleration measurements in space applications. The MESA is a space qualified instrument and has been employed in a number of successful space missions including NASA's Atmosphere Explorer and SERT 2 and the Air Force's 573-5, Cannon Ball 1 and 2, and SPADES.

Bell Aerospace's experience in the operation of a number of instruments in which a capacitive type pickoff is employed, is that the instrument resolution is limited by self generated noise within the sensor itself and in the associated electronics. It is the self generated noise that is of prime concern in the selection of an accelerometer for a satellite version of a rotating accelerometer gradiometer. It is not surprising that analysis shows that pendulous type accelerometers used successfully in a terrestrial rotating accelerometer gradiometer is not suited to the satellite version where 0.03 EU (10 sec time constant) or better performance is required. Preliminary analysis of noise from MESA's indicate that instrument and system noise consistent with performance requirements can be met.

Instrument and system self generated noise is analysed in Section 4.2 of this report, and indicate one, perhaps two, necessary modifications of the standard production unit. Further detailed analysis might reveal some minor desirable dimensional changes of such parameters as gap lengths. None of these modifications impact on the basic qualified instrument design, a description of which follows.

The proofmass, consisting of a thin-walled cylinder with a thin central flange, is electrostatically suspended by the application of voltages to the electrodes mounted to a carrier fitted inside the cylinder. Suspended against any cross acceleration forces, the proofmass is free to move along the cylinder axis (the input or sensitive axis).

Forcer assemblies are positioned on either side of the proofmass central flange. Each forcer assembly contains three concentric ring electrodes. The central ring electrode is used in a capacitive pickoff system to detect the position of the proofmass along the input axis. The two outer electrode rings are used to generate the rebalance forces to oppose the inertially induced forces from the accelerations to be measured.

The operation of the force rebalance system is shown in block diagram form in Figure 17.

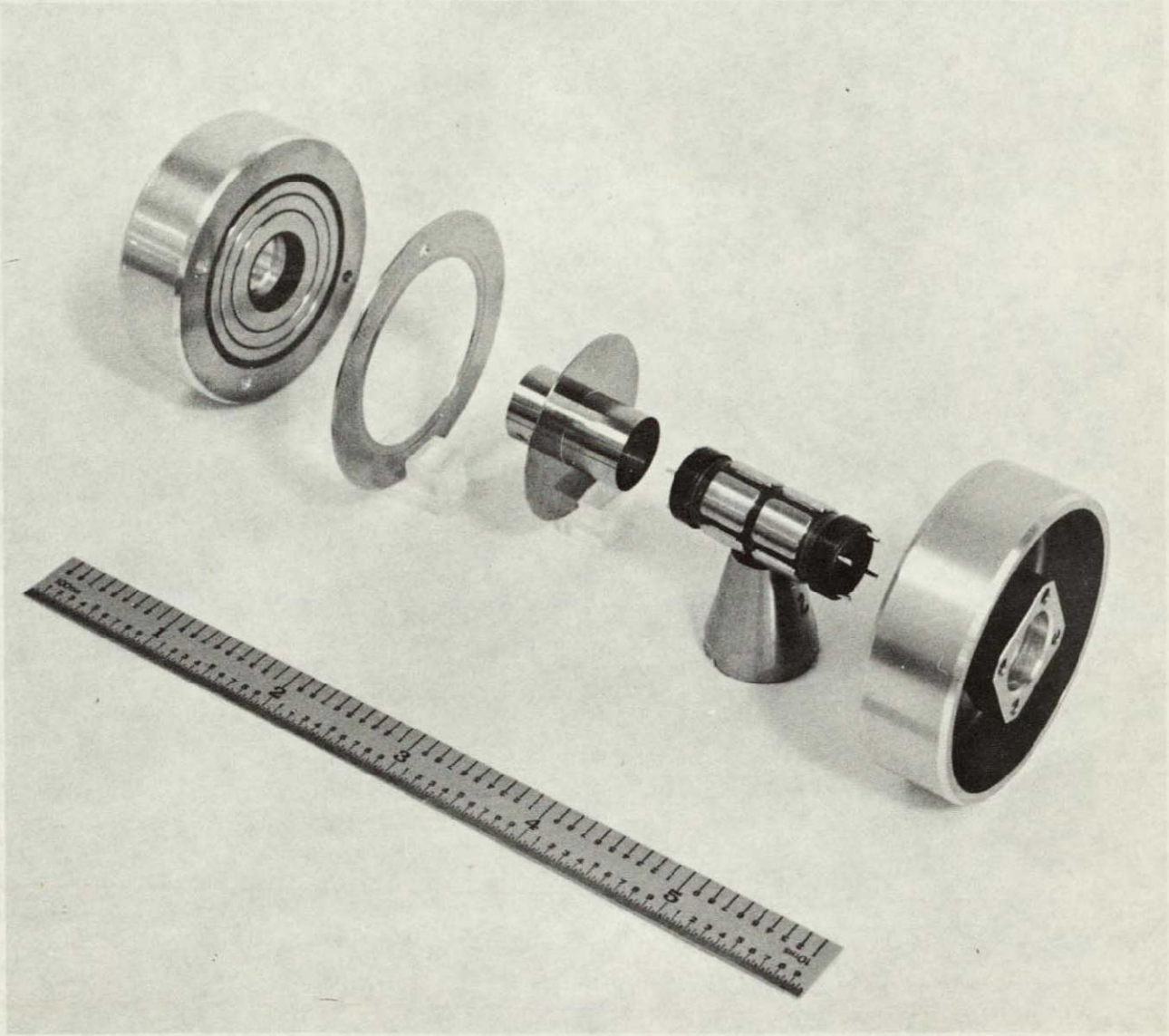

Figure 16. Bell Miniature Electrostatic Accelerometer (MESA)

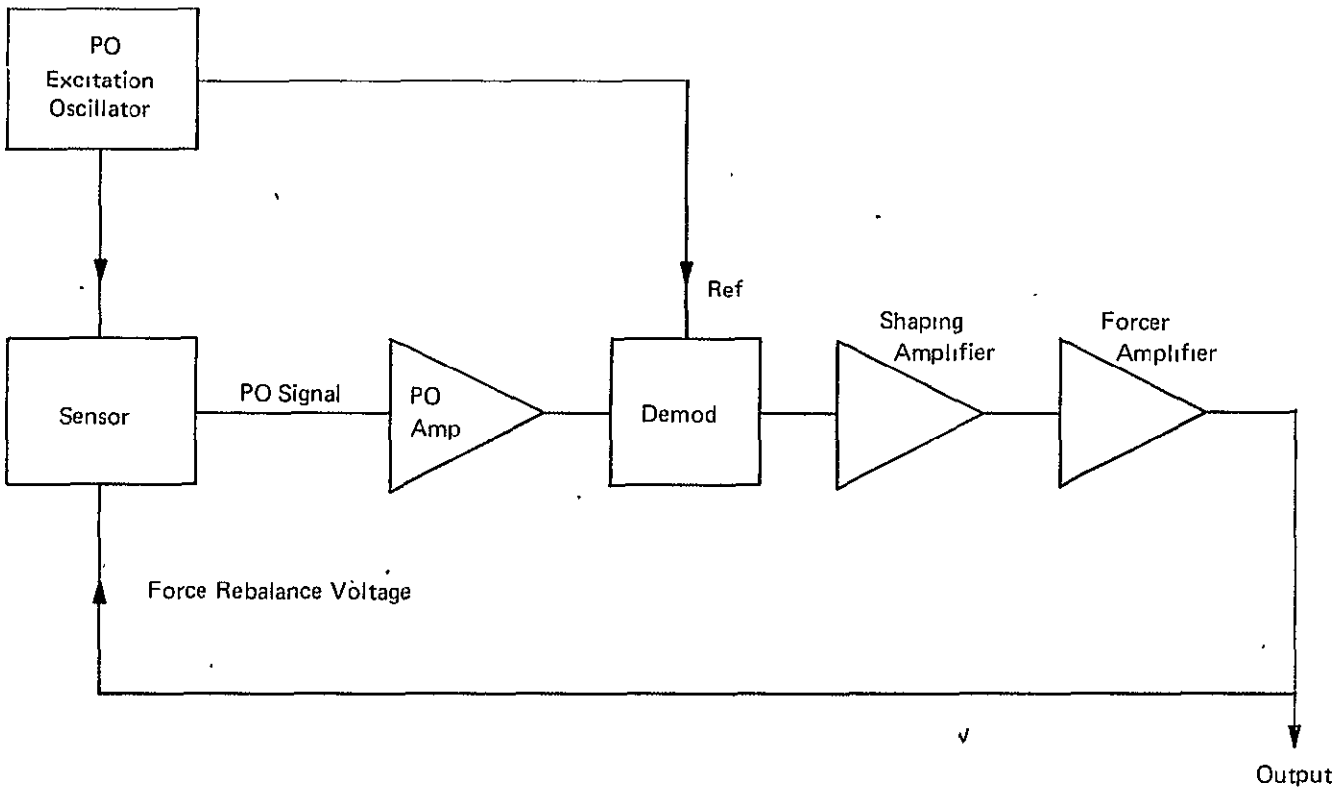

Figure 17. Block Diagram MESA Constrainment Loop

The capacitive pickoff is energized from an oscillator typically operating at 100 kHz. The pickoff output signal which defines the proofmass position by amplitude and phase is amplified and demodulated. The signal is then suitably shaped for loop stability and the desired frequency response before being amplified for application to the forcer electrodes. The action of the loop is thus to constrain the proofmass along the input axis to the null of the pickoff system.

Figure 18 (a) shows the most commonly implemented method of operating the capacitance pickoff system. The pickoff electrode to proofmass flange capacitances C_2 are connected in a bridge with fixed capacitances C_1. The bridge is excited by a voltage V_p at 100 kHz. The bridge output is fed to a differential amplifier prior to demodulation.

Figure 18 (b) shows the voltage applied to the forcer electrodes to generate the rebalance force. The reference voltage E_R is continuously applied and is basically used to linearize the instrument output. The voltage V is the voltage applied from the forcer amplifier to satisfy the constrainment loop. This voltage, or a multiple of the voltage, is the instrument output proportional to input acceleration. The voltage polarities are organized to maintain a net zero summed voltage with respect to the proofmass. Both E_R and V are dc voltages so that the instrument output is an analog dc voltage.

The electrostatic suspension of the proofmass against across axis acceleration forces is usually accomplished with a simple passive circuit. This suspension system can be scaled to permit instrument test on Earth in a 1g cross field. In a recent program, analog constrainment with a loop essentialy indentical to the input axis for the orthogonal cross axis has been developed to yield a 3 axis measuring instrument. For reasons explained in the noise analysis, analog constrainment in the cross axes will be necessary though not in a measurement mode.

It is estimated that a single MESA complete with its associated electronics will occupy about 100 $in.^3$ weigh about 4 pounds and consume about 6 watts.

4.2 Self Generated Instrument and System Noise

This section is devoted to self generated noise, and does not consider noise and errors generated by other spacecraft running equipment or undesired spacecraft motions, which are covered in Section 4.3. However, one aspect of the environment, namely steady deceleration (drag) or acceleration of the spacecraft, does impact directly on the self generated noise and has to be considered here. Sources of self generated noise can be broken down into three categories.

(1) True thermal noise (Brownian motion) in the MESA sensor unit.

(2) Electronic noise in the circuits directly associated with the operation of the MESA.

(3) Electronic noise in the circuitry associated with signal detection and interfacing with the spacecraft data transmission system.

The preliminary analysis results given are for a 4 MESA unit system, with each sensor at a nominal radius of 30 cm. This yields a scaling sensitivity of 4.2×10^{-11} g rms per EU for the cross gradient channel. The EU noise figures calculated are for a 10 sec time constant filter and apply to the lower sensitivity in-line gradient channel. The figures should be halved for the cross gradient channel.

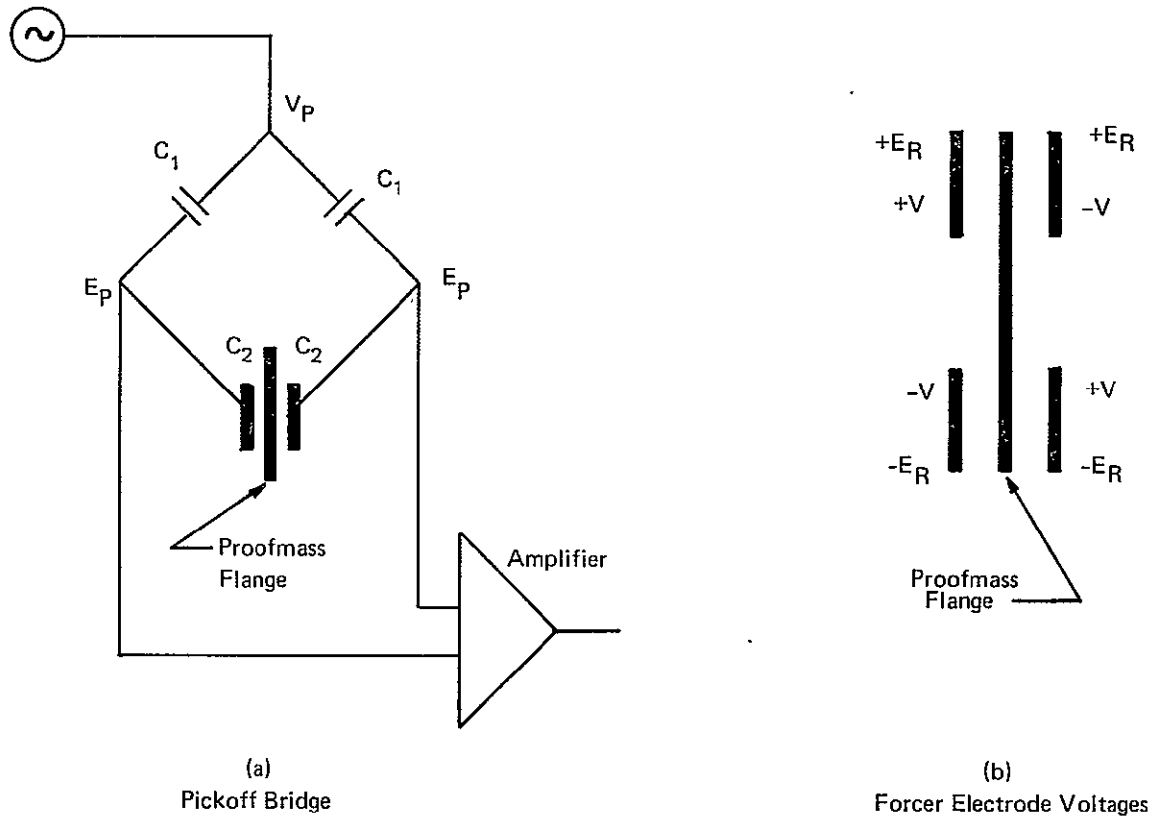

Figure 18. Pickoff and Forcing Arrangement

4.2.1 MESA Sensor Unit Thermal Noise

Since the MESA is essentially a force measuring device designed to measure inertially induced acceleration forces acting of the proofmass, the instrument will indicate all forces acting on the proofmass including those not inertially induced. There are two mechanisms for thermally agitated forces acting directly on the proofmass within the sensor unit itself. These are:

(1) Random collision of gas molecules with the proofmass.

(2) Random electron flow in the proofmass reacting with any magnetic field which is present.

The magnitude of these forces is related to the viscous damping coefficient associated with the mechanism; gas damping, and eddy current damping respectively for (1) and (2) above, by the following equation:

$$f_{rms} = \sqrt{4\,kTc\,\Delta f} \quad \text{dyne} \tag{22}$$

where

k = Boltzmann's constant in ergs/°K

T = Temperature in °K

c = Viscous damping coefficient in dyn/cm per sec

Δf = Bandwidth in Hz.

The validity of this equation has been proven experimentally in testing conducted on pendulous type accelerometers used in the terrestrial version of the Bell Rotating Accelerometer Gradiometer.

Equation (22) defines the total force noise, so that at a specific phase corresponding to one of the gradiometer output channels, and for a MESA proofmass weight of 1 gram, the acceleration noise from one sensor per channel is given by:

$$g_{rms} = \frac{\frac{1}{\sqrt{2}}\sqrt{4kTc\,\Delta f}}{981} \tag{23}$$

Since noise from four sensors adds on a rss basis, the noise from a pair of sensors increases to:

$$g_{rms} = \frac{2\sqrt{4kTc\,\Delta f}}{981\sqrt{2}} = \frac{\sqrt{8kTc\,\Delta f}}{981} \tag{24}$$

Ideally, the noise contribution from this source should be designed to be small with respect to 0.03 EU. Solution of equation (24) for a noise contribution of 0.01 EU yields a maximum allowable value of c to be 3×10^{-5} dyn/cm per sec, when the following parameters are used:

$k = 1.38 \times 10^{-16}$

$T = 300$

$\Delta f = 0.1$ rad/sec = 0.016 Hz (10 sec time constant filter)

$g_{rms} = 4.2 \times 10^{-13}$

Very rough preliminary calculations indicate that to achieve this level of viscous damping from the gas contribution, the sensor unit internal gas pressure, assuming air, should not exceed 4×10^{-6} torr.

For any eddy current damping, the presence of a magnetic field oriented orthogonal to the input axis combined with a gradient along the input axis is required. There will be no eddy current damping from a perfectly uniform field so that it is the field gradient which is significant. Very rough preliminary calculations indicate that to achieve the desired level of eddy current damping, the field gradient should not exceed 0.8 gauss/cm.

Restricting the magnetic field gradient to about 1 gauss/cm at the sensor location should not present any problems. Any problem that should arise in this area can be easily dealt with by adding magnetic shielding to the sensor or possibly by changing the proofmass material from beryllium to a higher electrical resistivity material.

Achieving a sensor internal pressure of 4×10^{-6} torr does raise a potential problem. It is believed that pressure this low could not be achieved and maintained in the standard hermetically sealed design. Two possible solutions that require further investigation are either venting the sensor in space or employing ion pumps in conjunction with sealed sensor units.

4.2.2 Constrainment Loop Electronic Noise

Electronic noise in the components of the constrainment loop causes forced motions of the proofmass by the action of the closed loop. If these forced motions could take place without any resultant forces acting on the proofmass, then noise in the constrainment loop electronics would not cause noise in the output. There are, however, two sources of forces acting on the proofmass from imposed motions. They are:

(1) Forces from negative spring rates to proofmass displacement due to electrostatics.

(2) Forces from the proofmass inertia.

Negative spring rates to proofmass motion along the input axis stem from voltages applied to both pickoff and forcer electrodes. The equation defining the spring rate is:

$$\frac{dF}{dx} = \frac{1.76 \times 10^{-6}\ AV^2}{d^3} \text{ dyn/cm} \qquad (25)$$

where

A = electrode area in cm^2

V = applied voltage in volts rms

d = gap length in cm.

Substituting the nominal values for a standard MESA yields the following:

$$\text{Pickoff spring rate} = -5 \times 10^{-3} \text{ g/cm per volt}^2 \tag{26}$$

$$\text{Forcer spring rate} = -1 \times 10^{-2} \text{ g/cm per volt}^2 \tag{27}$$

The inertia forces resulting from imposed motions can also be expressed as an effective spring rate at the frequency of interest.

$$\text{Inertia spring rate} = -\frac{(2\,\Omega)^2}{981} \text{ g/cm} \tag{28}$$

where

Ω = rotation angular frequency in rad/sec.

In order to assess the magnitude of the output noise from the constrainment loop electronic noise, it is necessary to establish the amplitude of the electronic noise referred to the preamplifier input. Knowing the pickoff gain at this point, the amplitude of the imposed motions can be calculated. It is then a matter of optimizing the operating voltages to minimize the output noise and determining any limiting environmental conditions.

The most significant contributor to noise in the constrainment loop electronics is the first amplifier, usually referred to as the preamplifier. It is noise about the operating frequency of 100 kHz that is of concern in this stage. In subsequent stages it is the noise at the frequency of interest that is significant. Using the best low noise component currently available and assuming the preamplifier stage is operated with a gain of 80 volts/volt, the calculated rms voltage noise referred to the preamplifier input as a function of frequency as seen through a 0.016 Hz bandwidth is plotted in Figure 19.

The gain through the pickoff bridge (at the input to the preamplifier) is known at 10 volts/cm per volt of bridge excitation.

The foregoing spring rate equations, constrainment electronic noise voltage and pickoff gain, permit calculation of output noise. There remains the optimum selection of two parameters, viz. the magnitude of the bridge excitation voltage V_P and the forcer reference voltage E_R. The factors which have to be considered in optimizing this selection are listed as follows:

(1) The pickoff bridge gain is proportional to $\frac{V_P}{d^2}$ while the pickoff electrode negative spring rate is proportional to $\frac{V_P^2}{d^3}$. Therefore the ratio of $\frac{\text{gain}}{\text{spring rate}}$ is proportional to $\frac{d}{V_P}$ and for a given d, noise associated with the pickoff electrode spring rate is minimized by the selection of a low V_P. However, a low V_P means large motion since the motion is simply $\frac{\text{noise}}{\text{gain}}$, and these large motions are undesirable because of the forcer and inertia spring rates.

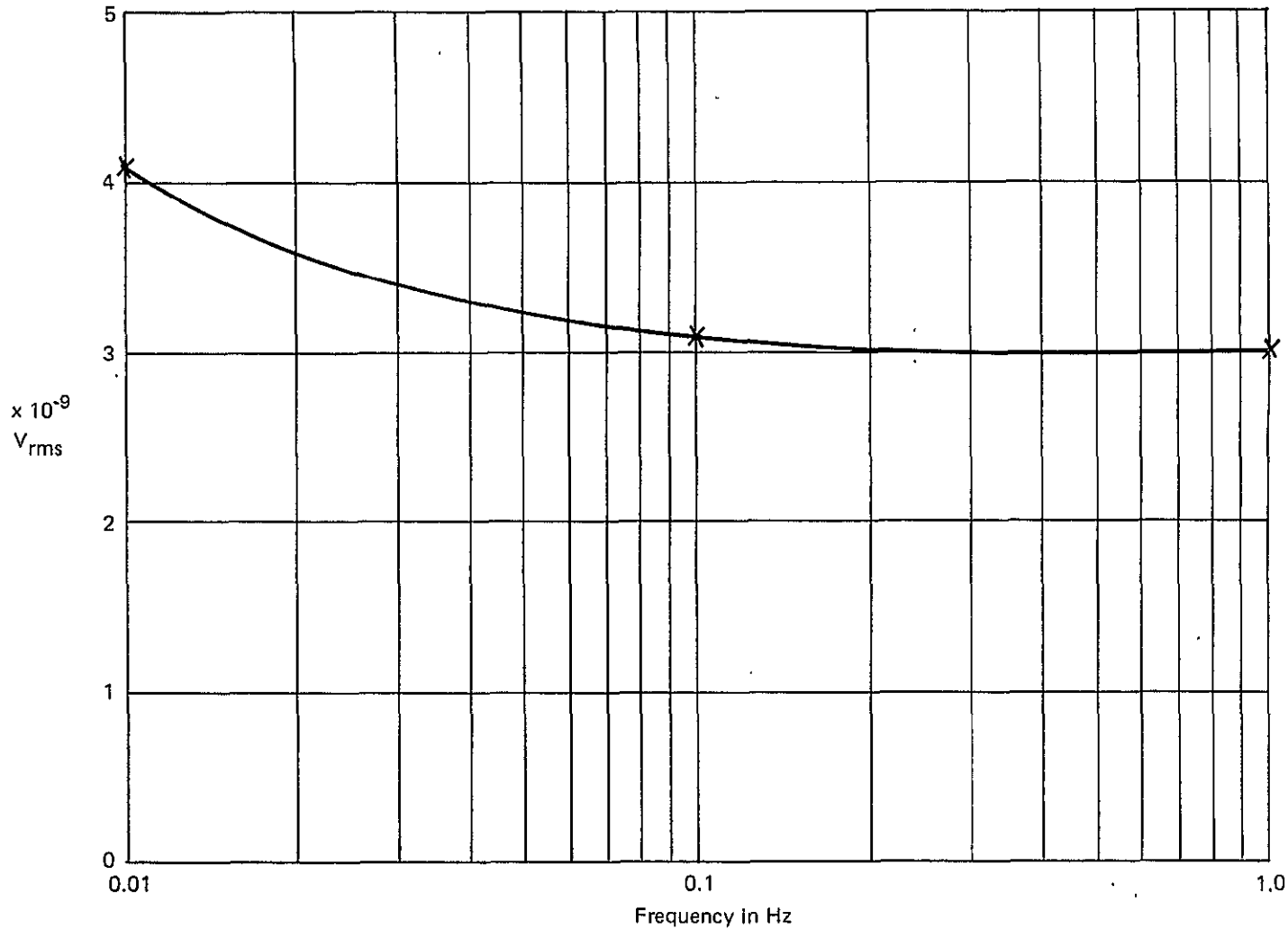

Figure 19. Constrainment Loop Voltage Noise Referred to Preamplifier Input

(2) The linear component of the rebalance force is proportional to $E_R V$. Therefore the lower E_R, the higher is V for a given g input. The voltage E_R is continuously present resulting in a constant spring rate and constant magnitude noise contribution. The value of V, being proportional to the input g, generates a spring rate, proportional to g^2 and consequently a magnitude of noise proportional to the square of the input g.

(3) The second order non-linearity error coefficient K_2 (in g/g^2) is proportional to $\frac{k_a}{E_R{}^2}$ where k_a is an asymmetry factor.

(4) The dc bias K_0 (in g) is proportional to $K_a(E_R)^2$. Although the dc bias is not directly of concern in the gradiometer application, a parameter such as the bias temperature coefficient is also proportional to $K_a (E_R)^2$ and hence sensitivity at 2 Ω to any 2 Ω temperature variations.

(5) The effective negative spring rate from the proofmass inertia is negative and therefore additive to the electrostatic spring rates. As the frequency of rotation is increased, this inertia spring rate becomes progressively more significant with respect to the electrostatic spring rates, requiring larger V_P for small motions for optimum conditions.

Although the second order non-linearity and dc bias considerations cannot be ignored, preliminary investigation indicates that these aspects are unlikely to influence the selection of E_R. It is noise that is by far the most significant factor influencing the selection of E_R.

A parametric study can be conducted to show the noise in the gradiometer output from electronic noise in the constrainment loop as a function of angular rotation frequency Ω and g input (for example satellite drag and centripetal acceleration from rotation coupling in from tangential misalignment) for different selections of V_P and E_R. Two examples are shown in Figures 20 and 21, where the 1σ EU plotted is the noise level as seen through a 10 second time constant filter. It is clear that from constrainment loop noise considerations, the lower the input g and the rotation frequency, the lower will be the noise contribution. There is a secondary advantage here in that low input g and rotation rates permit the selection of low values for V_P and E_R. Not only do these voltages generate a negative spring rate but also a net force if an asymmetry condition exists. Noise on V_P and E_R from the electronics generating these reference levels can potentially lead to problems if the nominals and asymmetry conditions are high.

4.2.3 Suspension Electronics Noise

The requirement to vritually eliminate gas damping in the input axis from thermal noise considerations, also eliminates damping in the two orthogonal suspension axes. A passive suspension scheme is therefore not practical. The proofmass will be suspended by the use of an analog constrainment loop similar in principle to the input axis constrainment loop. In this case a common electrode will be used for both the pickoff and forcing function. A MESA development program is currently underway to implement such a scheme for the purpose of achieving a 3 axis measurement instrument. It has already been demonstrated that constrainment by this technique is practical.

The areas of concern for electronic noise in the suspension electronics are twofold:

(1) Electronic noise in the suspension constrainment loop electronics will cause proofmass motions along the suspension axis. The potential exists for these motions to cross couple into the input axis pickoff system causing input axis motions.

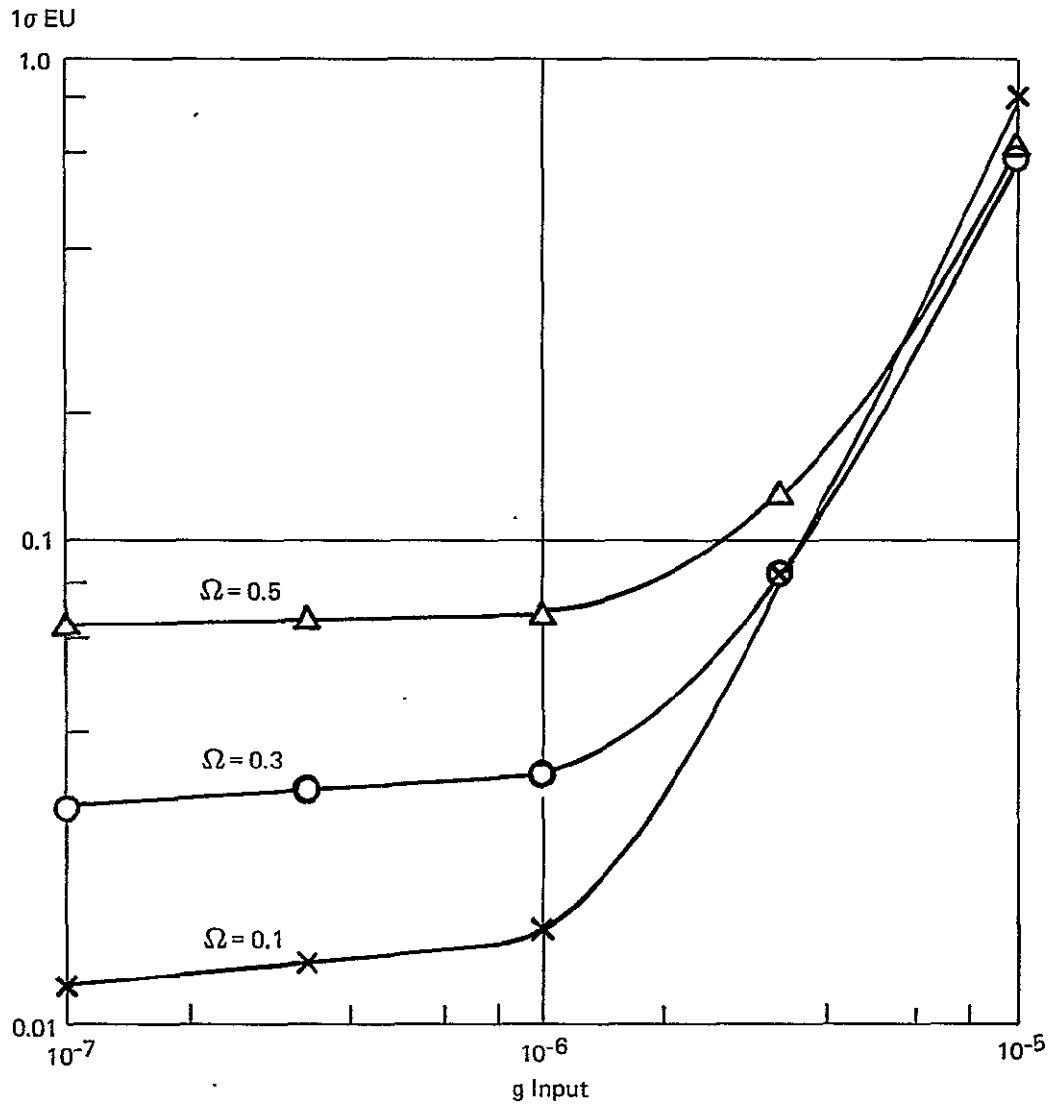

Figure 21. Constrainment Loop Noise $V_P = 0.25$, $E_R = 0.05$

(2) The application of pickoff and forcing voltages to the suspension electrodes potentially cause forces to cross couple into the input axis through some asymmetry condition. In addition, the voltage application could generate a small negative spring rate along the input axis due to certain geometric asymmetries.

With regard to the motions along the suspension axis, since the pickoff gain is actually larger due to a shorter gap length, the motions should certainly be limited to no greater than those in the input axis due to its own constrainment loop. Even if as large a coupling as 1% existed (0.01 to 0.001% is more likely) this effect can be expected to be negligible.

The only significant acceleration input against which the proofmass has to be suspended is the centripetal acceleration from rotation. At Ω of 0.1 rad/sec, this acceleration is roughly 3×10^{-4} g at a radius of 30 cm. Forcing voltages for this g input level will only be in the 1 or 2 volt region so that a negligible contribution to input axis stiffness will result. This assessment is based on experimental measurement with 100 to 200 volt application required to suspend against the full earth's g. The force noise in the suspension axis (10 second time constant) for a 3×10^{-4} g input can be calculated by the same method used for the input axis, and can be shown to be roughly 2×10^{-11} g. Cross coupling of forces from suspension axis to input axis is typically 3×10^{-5} g/g so that the cross coupled noise is roughly 6×10^{-16} g which is negligible. Even at an $\Omega = 1.0$ rad/sec this cross coupled force noise increases by a factor of 100 to about 6×10^{-14} g per sensor or roughly 1×10^{-13} g for a pair of sensors contributing 0.005 EU to the gradiometer noise.

This preliminary analysis indicates that for angular rotation frequencies of 1.0 rad/sec or less the contribution of noise from the suspension electronics is negligible.

4.2.4 Signal Detection Electronic Noise

The signal detection and processing electronics consists of the basic elements are shown in Figure 13. The most significant noise contributor is the bandpass amplifier, this stage being at the lowest signal level point. High gain in this stage renders noise in subsequent stages negligible. Using the best low noise amplifiers currently available, the rms voltage noise at this amplifier input as seen through 10 sec time constant filter as a function of frequency is shown in Figure 22.

The voltage scaling of the standard MESA output is a function of:

(1) Value of E_R selected,

(2) Max voltage swing capability of the constrainment loop forcer amplifier, the signal level attenuation before application to forcer electrode, and the maximum constrainment g level required.

The noise contribution from the detection electronics as seen through a 10 second time constant filter as a function of rotation angular frequency is shown in Figure 23 for the following assumptions.

$E_R = 0.1$ volts

Forcer Amplifier Swing 30 volts max.

Signal level attenuation of 10 leading to a maximum constrainment capability of 6×10^{-5} g.

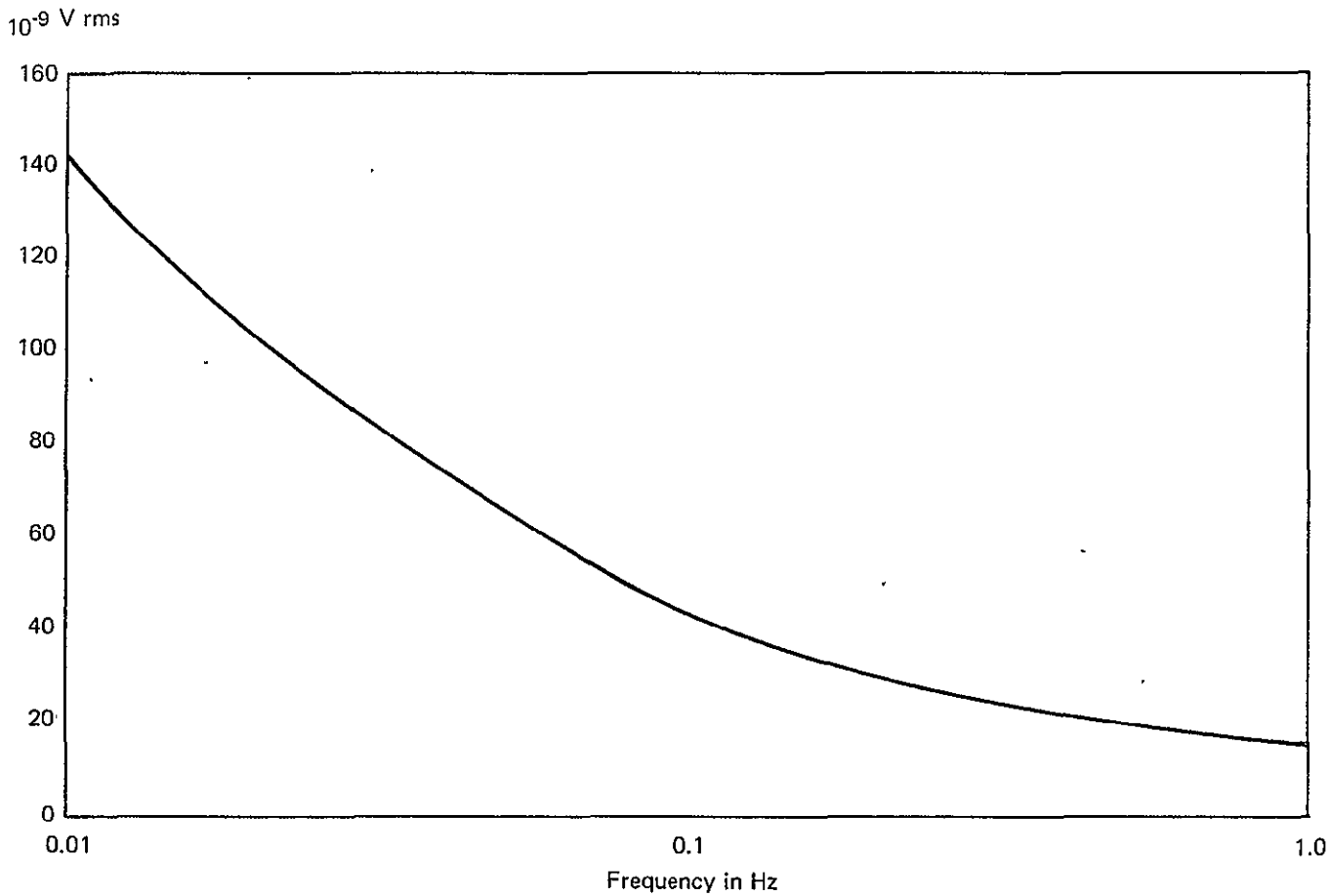

Figure 22. Detection Electronics Voltage Noise

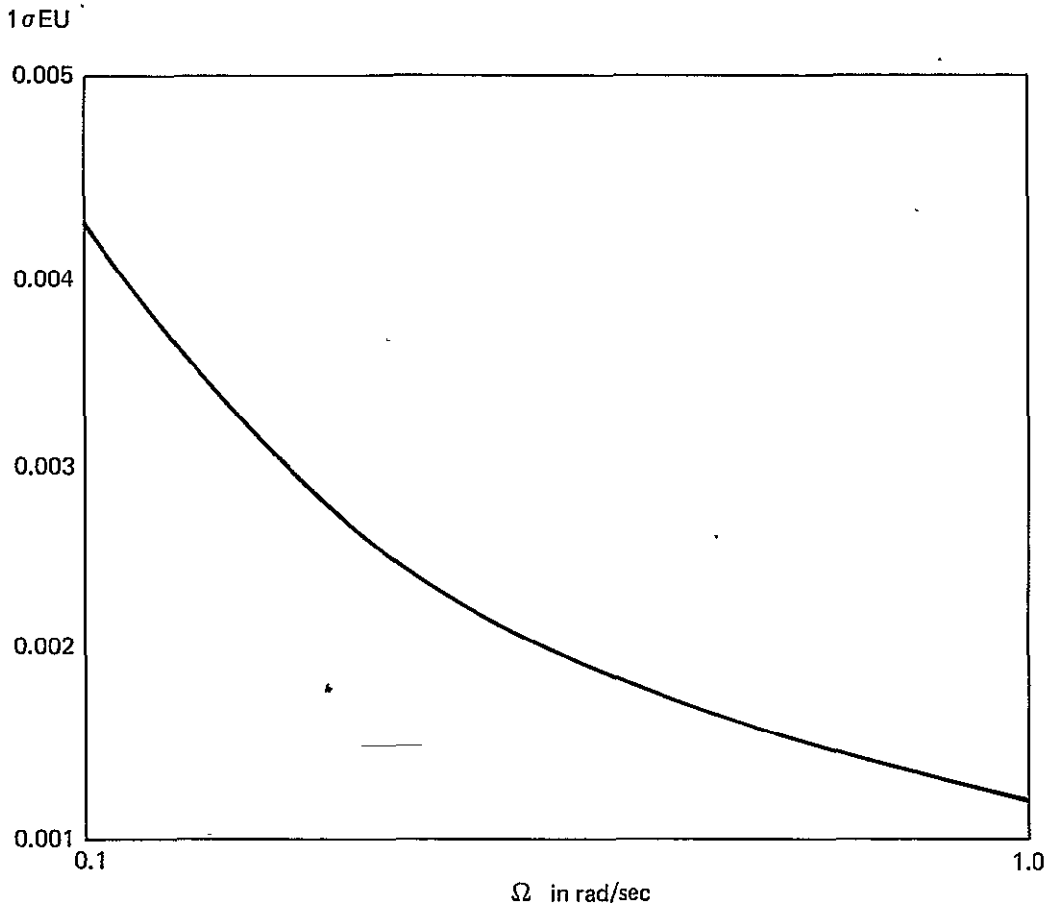

Figure 23. Signal Detection Electronic Noise

Since high gain in the detection electronics renders noise in subsequent stages relatively insignificant, it is not expected that interface electronics will present a noise problem.

4.3 GRADIOMETER SPACECRAFT INDUCED ERROR SOURCES

For a perfect spinning system in a perfect environment the only source of gradiometer error will be self generated noise. Compared to a terrestrial spinning mechanism in a 1g environment, the spinning orbital vehicle approaches the perfect system. However, there will be imperfections and some of these imperfections result in gravity gradient measurement errors.

Without detailed knowledge of the spacecraft characteristics, a full error analysis is clearly not practical at this time. Such an error analysis could only be conducted in a study phase in close cooperation with NASA and spacecraft personnel. However, there are a number of considerations relating to the spacecraft which are clear from the analysis of gradiometer errors. Some of these considerations may be specific to the Bell gradiometer employing rotating accelerometers, while some will apply to any gradiometer system. This section is devoted to a discussion of these considerations.

In the consideration given to error sources, it should be borne in mind that the prime objective of the gradiometer is to measure the higher harmonic degrees of the earth and particularly haromincs in the band of about the 10th to 100th. Ideally, the gradiometer accuracy should be extended to the lowest possible harmonic to give a maximum overlap with harmonic data obtained from doppler tracking for correlation. From white noise considerations, the doppler tracking method is superior to the gradiometer at the lower harmonics of the earth and certainly below the 10th. The errors sources considered in this section are not white, and in general can be thought of as a bias output. An error mechanism generating a constant bias would be no concern. It is variations over an orbit of a bias producing error mechanism that is of importance. With an orbit time of about 90 minutes the 10th harmonic has a period of about 9 minutes and the 100th of about 54 seconds. Bias variations outside this frequency range do not impact on the prime mission of the gradiometer. This is an important consideration and will be emphasized on more than one occassion in the following subsections.

4.3.1 Spacecraft Drag

Drag deceleration potentially impacts on the gradiometer performance in a number of ways. As shown in the preliminary analysis of self generated system noise, steady inputs must be limited to a few micro g. It is possible that this aspect is the most significant consideration with respect to drag deceleration.

The drag deceleration will be seen in each MESA modulated at the spin frequency (1 Ω). Second order error coefficients potentially give rise to errors at the gradiometer detection frequency of twice spin frequency (2Ω).

Just considering the second order non-linearity coefficient K_2, an error term is generated given by

$$\frac{\frac{1}{2} a^2_d \Sigma K_2 \cos 2\Omega t}{1.2 \times 10^{-10}} \quad \text{EU} \quad \cdots$$

where a_d = drag deceleration in g

ΣK_2 = sum of second order non-linearity coefficients in g/g^2.

It will be seen that the error term contains a_{d^2} so if a_d is limited to about 3×10^{-6} g by selection of a suitable orbital attitude, ΣK_2 would have to be very large before a significant error developed. The second order non-linearity coefficient is proportional to $\frac{k_a}{E_{R^2}}$ where k_a is an asymmetry factor. Prior experience indicates that unless E_R is selected at an unreasonably low value, this error source will be negligible for values of a_d in the few micro g range.

Asymmetry in the spacecraft profile can react with the drag deceleration to generate a spin frequency harmonic component in the drag deceleration and in a modulation of the spin frequency. Of concern is the 1Ω component of deceleration and 2Ω modulation about the spin axis.

The 1Ω content of the drag deceleration is modulated at 1Ω by rotation and appears at the MESAs as a 2Ω acceleration. This signal is rejected in the summed output of the MESAs within the scale factor balance of the pairs. The automatic scale factor balancing described in Section 3.0, block diagram Figure 14 is specifically designed to render this particular error mechanism to be negligibly small.

Angular modulation about the spin axis causes tangential accelerations to appear directly in the MESA input axes, and centripetal accelerations to couple into the MESA input axes by the tangential misalignment of the sensors. In the terrestrial version of the gradiometer this particular error source is minimized by a combination of a set up on test procedure and an automatic sum of pairs scale factor balance loop. This involves the deliberate introduction of a modulation about the spin axis at a discrete frequency close to but not harmonically related to the spin frequency. Such a scheme may not be beyond the wit of man in the orbital spacecraft application, but is clearly undesirable and in any case may well not be necessary.

For a modulation angle about the spin axis of θ peak radians, the tangential and centripetal acceleration is given by

$$a = \frac{\theta.R.(2\Omega)^2}{981} \text{ g}$$

The gradiometer error signal is given by

$$e = \frac{k.\theta.R\,(2\Omega)^2}{981 \times 6 \times 10^{-11}} \text{ EU}$$

where k = rejection factor
R = radius arm of accelerometer, cm
Ω = spacecraft rotation frequency

If a rejection factor k of 0.0025 is assumed together with an Ω of 0.2 rad/sec then a 0.03 EU error will be generated by a modulation angle of 1.5×10^{-7} radians.

The assumed rejection factor of 0.0025 is based on the accuracy of the scale factor balance between the summed pairs and on the net tangential alignment of the four sensors. The accuracy of the scale factor balance is dependent not only on the instrument scale factor in volts/g but also on the separation distance between the pairs of accelerometer sensors. Achieving instrument scale factor match to 2.5 parts in 1000 is easy, and controlling the separation distance to that involves positioning of the sensors a nominal 60 cm apart to an accuracy of 1.5 mm. More difficult to achieve is the tangential alignment since this requires knowledge of center of rotation of the spacecraft.

Although not related to drag, the topic of this section, it is perhaps an appropriate point in the discussion to raise another requirement for tangential alignment. The constant rotation of the spacecraft generates a dc centripetal acceleration of about 1.2×10^{-3} g at a radius arm of 30 cm for a 0.2 rad/sec rotation frequency. This dc acceleration will couple into the input axis by tangential misalignment and is thus a potential contributor to self generated noise as explained in Section 4.2.2. To limit the acceleration to the desired maximum of about 3×10^{-6} g requires that the individual accelerometers be tangentially aligned to better than 0.0025 radians. This 0.0025 radian figure is consistent with the assumed rejection k of 0.0025 above.

Achievement of a 0.0025 radian tangential alignment in a 30 cm radius requires among other things, a knowledge of the center of rotation of the spacecraft to better than 0.75 mm. Prediction of the center of spacecraft roation to this accuracy is likely to prove impossible requiring that this problem be solved by a technique which does not involve rotation center prediction.

One possible practical solution is to incorporate in the MESA mount an electromechanical mechanism for changing the tangential alignment. Such a mechanism could either rotate the sensor or translate the sensor tangentially. The output of each MESA will give an accurate indication of its tangential alignment by the magnitude of the dc level. This dc level will contain the instrument bias, expected to be very small, in addition to the dc from tangential misalignment. With the spacecraft in orbit each MESA output can be monitored in turn, and on command the position servoed for a null dc output. This servo loop would not be continually activated because of noise generation, but activated at the start of the gravity gradient measurement mode. Should the center of rotation shift beyond 0.75 mm during the measurement mission (from fuel usage for example), the positioning system could be periodically reactivated on command.

4.3.2 Spacecraft Temperature

It is believed that temperature control of the MESA is highly undesirable from power usage considerations, and should not be necessary. Consideration has therefore to be given to the temperature environment of the spacecraft. Errors associated with temperature variations occurring specifically at a frequency of 2Ω, and to a lesser extent by 1Ω have to be assessed in addition to the impact of the ambient temperature.

Temperature variations at harmonics of the spin speed can certainly be expected from the radiant heat of the sun acting on a slowly spinning spacecraft. Temperature variations of the MESA occurring at 2Ω will react with the MESA bias temperature coefficient to generate a direct 2Ω error output. The bias temperature coefficient of the MESA is a function of the electrode voltages and for the proposed operating levels is predicted to be 2×10^{-10} per °C. Assumming uncorrelated coefficients, the error is given by

$$\frac{2 \times 2 \times 10^{-10}}{6 \times 10^{-11}} \text{ EU per deg C at } 2\Omega$$

$$= 6.7 \text{ EU per deg at } 2\Omega$$

A 0.03 EU bias would result from a 0.005°C variation at 2Ω. A modulation of any 2Ω temperature variation with periods in the 54 sec to 9 minute range of this magnitude would not seem very likely.

A temperature variation at 1Ω potentially impacts on the performance in two ways. First the 1Ω temperature variation reacts with the MESA bias temperature to generate a 1Ω signal not related to scale factor imbalance. Such a signal causes the automatic 1Ω scale factor balance loops (Block Diagram Fig. 14) to operate with an offset error. This error however, is assessed to be negligibly small.

Secondly and more importantly the 1Ω temperature variation reacts with the MESA scale factor temperature coefficient to change the scale factor at a 1Ω rate. This modulation reacts with the drag deceleration to generate a 2Ω error. If, for example, the scale factor is modulated at m sin Ωt, then an instrument seeing the drag deceleration modulated at sin Ωt, will have an output given by

$$\frac{a_d \sin \Omega t}{1 + m \sin \Omega t}$$

$$= \quad a_d \sin \Omega t + \tfrac{1}{2} m a_d \cos 2\Omega t + \ldots\ldots$$

The uncompensated MESA scale factor temperature coefficient is of the order of 200 ppm per deg C. Assuming correlated coefficients, the error term without compensation, is given by

$$\frac{4 \times \tfrac{1}{2} \times 2 \times 10^{-4} a_d}{6 \times 10^{-11}} \text{ EU per deg C at } 1\Omega$$

$$= \quad 6.7 \times 10^6 a_d \text{ EU per deg C at } 1\Omega$$

For a drag deceleration of 3×10^{-6} g this error term becomes 20 EU per deg C at 1Ω. Open loop temperature compensation can be implemented to operate with probably a 5% accuracy bearing in mind temperature gradients that will occur at the 1Ω frequency. This would reduce the sensitivity to about 1 EU per deg C at 1Ω yielding a 0.03 EU bias for 0.03 deg C temperature variation.

Probably thermal insulation in the mounting of the MESA from the spacecraft structure would considerably attenuate 1Ω temperature variations at the MESA itself. Again remembering that it is amplitude modulation of this 1Ω temperature variation in the 54 sec to 9 min periods that is of concern, it would seem likely that errors from this source will be small, but should be studied further.

The only impact on gradiometer performance from ambient temperature changes is to change the gradiometer scale factor i.e., the volts per EU. This potentially impacts on the performance of the in-line gradient channel $W_{xx} - W_{zz}$ because of the relatively large standing level of about 3900 EU. Gradiometer scale factor ambient temperature sensitivity can be expected from two main sources viz the scale factor sensitivity of the MESAs themselves and the temperature sensitivity of the radius arm. If the radius arm is part of the spacecraft structure, which would seem the most practical mechanical implementation, a temperature coefficient of up to 25 ppm per deg C is likely. Temperature compensation of the MESA together with correction for the spacecraft temperature would probably reduce the overall scale factor coefficient to a few ppm per deg C. Temperature gradients would most likely be the factor which limits the accuracy. With a nominal gradient of 3900 EU an 8 ppm scale factor change results in a 0.03 EU error. If the ambient temperature within the spacecraft is expected to be ±10 deg C then variations with periods of 54 sec to 9 mins might well be small. However, it is assumed that some form of temperature control is employed to maintain the spacecraft at ±10 deg C. The characteristics of any control will have to be considered for frequency content.

4.3.3 Spacecraft Spin Speed, Attitude, Precession Rates, and Nutation

As explained in Section 2.1, the minimum spin speed of the spacecraft is dictated by the data acquisition rate and the highest harmonic sought. To acquire the 100th harmonic degree requires 200 data points per orbit and with data acquisition at once per revolution this puts the minimum spin speed at a little over

0.2 rad/sec or roughly 2 rpm. Somewhat higher spin speeds, should they be desirable for other spacecraft reasons should not be ruled out. The biggest disadvantage for the gradiometer is the increased centripetal acceleration term. However, the proposed MESA tangential alignment mechanism, if adopted, should be able to tolerate larger centripetal accelerations than from the minimum acceptable spin speed. In some other error mechanisms, increased speed is an advantage e.g., 1Ω and 2Ω temperature variations.

The proposed self generated demodulation reference signal scheme eliminates the requirement for any additional pitch attitude information, makes the actual spin speed non-critical and tolerates slow changes in spin speed which can be expected from aerodynamic and magnetic despin torques.

The spin axis will be nominally orthogonal to the orbital plane, so that attitude-errors in roll and yaw have to be considered. In addition, angular rates about the roll and yaw axes generate acceleration gradients which the gradiometer promptly measures as it should, so that angular rates are a direct source of error.

For roll and yaw attitude errors, the gradient signals are attenuated by cosine of the double error angle:-

$$\text{In Line Gradient} = \left(\frac{W_{xx} - W_{zz}}{2}\right) \cos 2\phi$$

$$\text{Cross Gradient} = W_{xz} \cos 2\psi$$

where ϕ = roll misalignment angle

and ψ = yaw misalignment angle

Since the nominal value of W_{xz} is zero, the yaw error is not highly critical, but the nominal 3900 EU in the in line gradient renders roll misalignments very sensitive. For a 0.03 EU error cos 2ψ has to be known to an accuracy of about 8×10^{-6}. This suggests limiting the roll angle error to 0.12° or if the roll error is allowed to build up knowing the error angle to high accuracy - about 0.006° for 1° roll error, 0.003° for a 2° roll error. Again it is modulation of the roll attitude error in the 54 sec to 9 min period which is of concern, but in view of the high sensitivity this aspect requires further study.

The angular rate sensitivity is simply given by 1 EU per 10^{-9} $(\text{rad/sec})^2$. A 0.03 EU error will be generated by an angular rate of 5.5×10^{-6} rad/sec or about 1.1°/hr. Consideration will have to be given to the attitude control system in the light of this sensitivity.

Spacecraft nutation should be a true coning motion. Coning motion does not generate errors from the angular rates associated with the motion, so that nutation is not expected to be a problem area.

4.3.4 Spacecraft Magnetic Environment

The preliminary analysis of self generated noise indicated a requirement to limit the field gradient to 1 gauss/cm. The MESA performance is very insensitive to magnetic fields. A very small bias sensitivity can be predicted for a field orthogonal to the input axis with a gradient in amplitude along the input axis (same as self generated noise). Errors from this source should be negligible, but in any case can be easily dealt with by the addition of magnetic shielding to the MESA, if necessary.

4.3.5 Spacecraft Vibration

The potential exists for the MESAs to experience acceleration inputs from the vibrations transmitted through the spacecraft structure from other equipment aboard the spacecraft. Common mode inputs to all four MESA are rejected within scale factor balance and alignment accuracies. However, some equipment such as horizon scanners for example are likely to produce inputs which are not common mode. Since any vibration and noise producing equipment will be fixed with respect to the accelerometers of primary concern is the magnitude of vibration at and near 2Ω (about 0.4 rad/sec).

A vibration power spectrum which is flat in the region of 2Ω which couples into one accelerometer ONLY, of magnitude Φ g^2 per rad/sec will cause a gradiometer noise output of

$$\frac{\Phi}{(4.2 \times 10^{-11})} \ EU^2/rad/sec$$

Thus for a 0.01 EU^2/rad/sec accuracy (0.03 EU in 10 seconds), the value of Φ representing a non-common mode input cannot exceed about 18×10^{-24} g^2 per rad/sec. Although this is a very small density amplitude it is applicable to a very low frequency of 0.4 rad/sec. It is clear, however that further study in this area is required. Operating in the gravity gradient measurement mode between the poles with all noise producing spacecraft equipment shutdown may or may not be a feasible approach. Mounting of the accelerometers to a dedicated structure with careful design in the mounting of this structure to the spacecraft may well substantially reduce non-common mode inputs.

4.3.6 Spacecraft Orbital Height, Spin Speed and Attitude Corrections

The effect of aerodynamics and magnetic fields will require that periodic thrusting be applied to maintain orbital height, spin speed and attitude. The foregoing consideration of error sources suggest that performance degredation might be experienced when thrusting is activated. Passes over the earth poles will be made in each orbit. Use may be made of this fact in two possible ways. One is to use data acquired in each pass in a calibration mode. The other is to disregard gradient data acquisition while required thrusting is accomplished. Depending on how often such thrusting corrections are necessary, possibly a combination of the two advantages could be beneficially implemented.

5.0 STATUS OF ROTATING ACCELEROMETER GRAVITY GRADIOMETER DEVELOPMENT PROGRAM FOR SAMSO

A status report on the feasibility demonstration model of the rotating accelerometer is added to this report to substantiate the soundness of the approach and lend a high confidence factor of success to the orbital gravity gradiometer. The objective of the airborne feasibility model is to demonstrate a performance of 1 EU as measured in all attitudes and under dynamic conditions. The attitude most closely approaching the orbital case is a slightly off vertical rotation axis (minutes of arc) causing a small amount of acceleration to couple into the sensitive axis of the accelerometer.

For the initial test program a GFE precision rate table was used to furnish the rotating fixture. The photograph, Figure 24, illustrates the setup. The four Model VII accelerometers can be seen mounted to the instrument block. The constrainment electronics and the detection electronics is mounted on vector board with each component available for troubleshooting and investigative testing

In the background is the 100 kgm gradient inducer which can be traversed on an overhead rack for calibration purposes.

The block diagram, Figure 25, illustrates the signal flow. The four accelerometers a_1 through a_4 are schematically shown with their constrainment electronics E_{a_1} through E_{a_4} on the rotating fixture indicated by the circle. The four constrainment currents are summed and amplified by the detection electronics prior to being passed through slip rings. The output of the detection electronics is demodulated at sine $2\Omega t$ and cos $2\Omega t$ and passed through ten second filters. These are the outputs of the gradiometer which are displayed on an analog strip chart and digitally tape recorded for computer analysis. The output of the detection electronics is demodulated also at sin Ωt, cos Ωt and sin $\omega_s t$ to establish the scale factor unbalance of the accelerometers. These signals are integrated and currents generated into the scale factor adjustment coils. ω_s is the angular modulation frequency imposed in the spin speed of Ω to permit detection of scale factor unbalances between the summed pairs of accelerometers.

The output of individual accelerometers are also passed through slip rings for diagnostic purposes. One accelerometer output is demodulated at sin Ωt and cos Ωt to indicate the off vertical tilt of the rotation axis.

The chart on Figure 26 gives the typical performance figures of an overnight run. An HP 830 computer continuously records the output of both channels of the gradiometer and on-line analyses 128 consecutive 10 second average data points for mean (bias, trend (change of bias with time)) and randomness around a best fit straight line.

The randomness of 80 blocks of 128 data points is 1.07 EU with the worst reading and best reading not exceeding ±20% of that value.

The bias of 40 consecutive data blocks exhibits a one sigma randomness of less than 0.4 EU with negligible trend for an overnight run. The overnight bias stability for the 40 data blocks of each gradiometer output channel is plotted on Figure 27. The excellent bias characteristics for an overnight run without temperature control is indicative of the soundness of the approach.

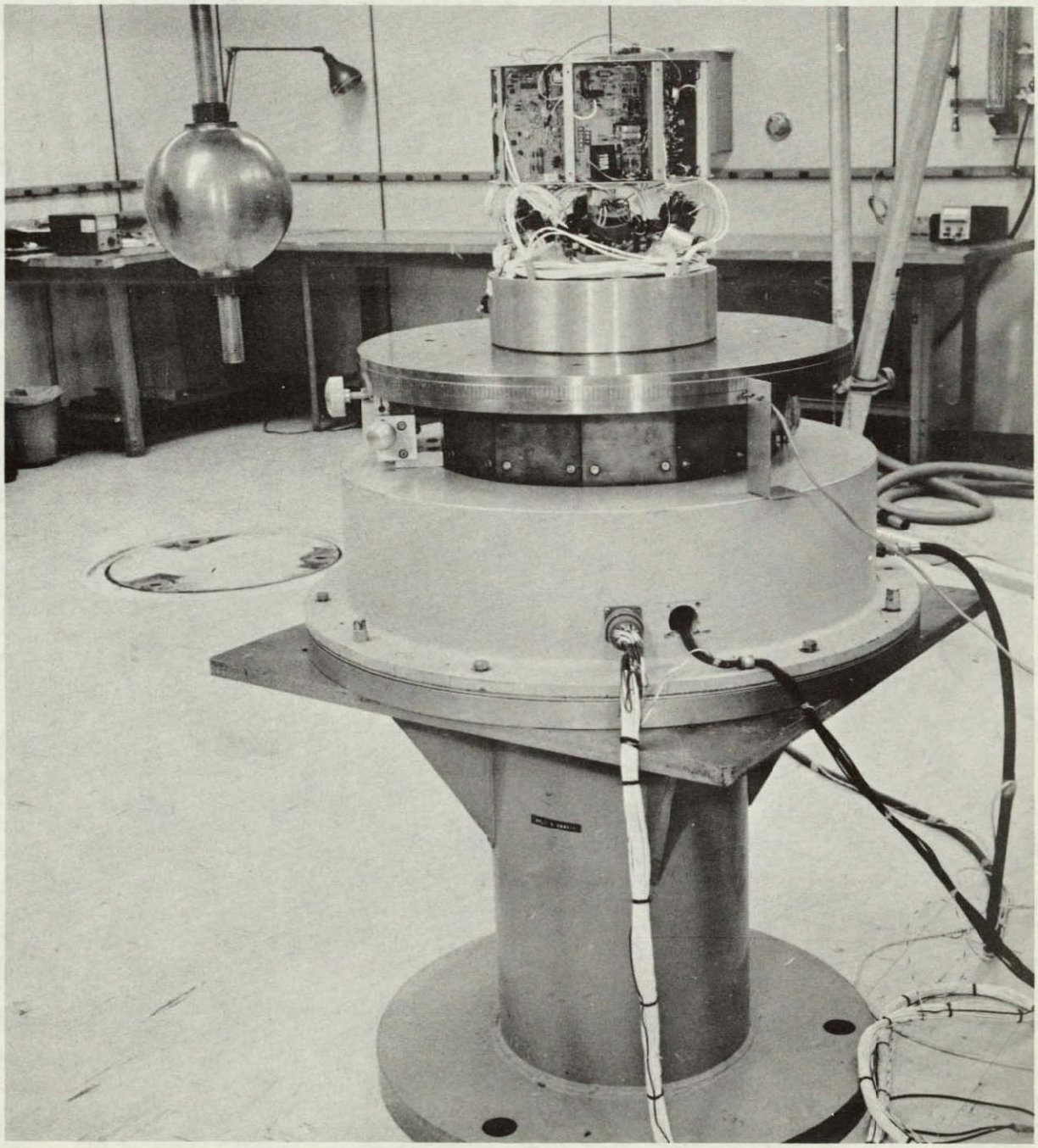

Figure 24. Rotating Accelerometer Gravity Gradiometer

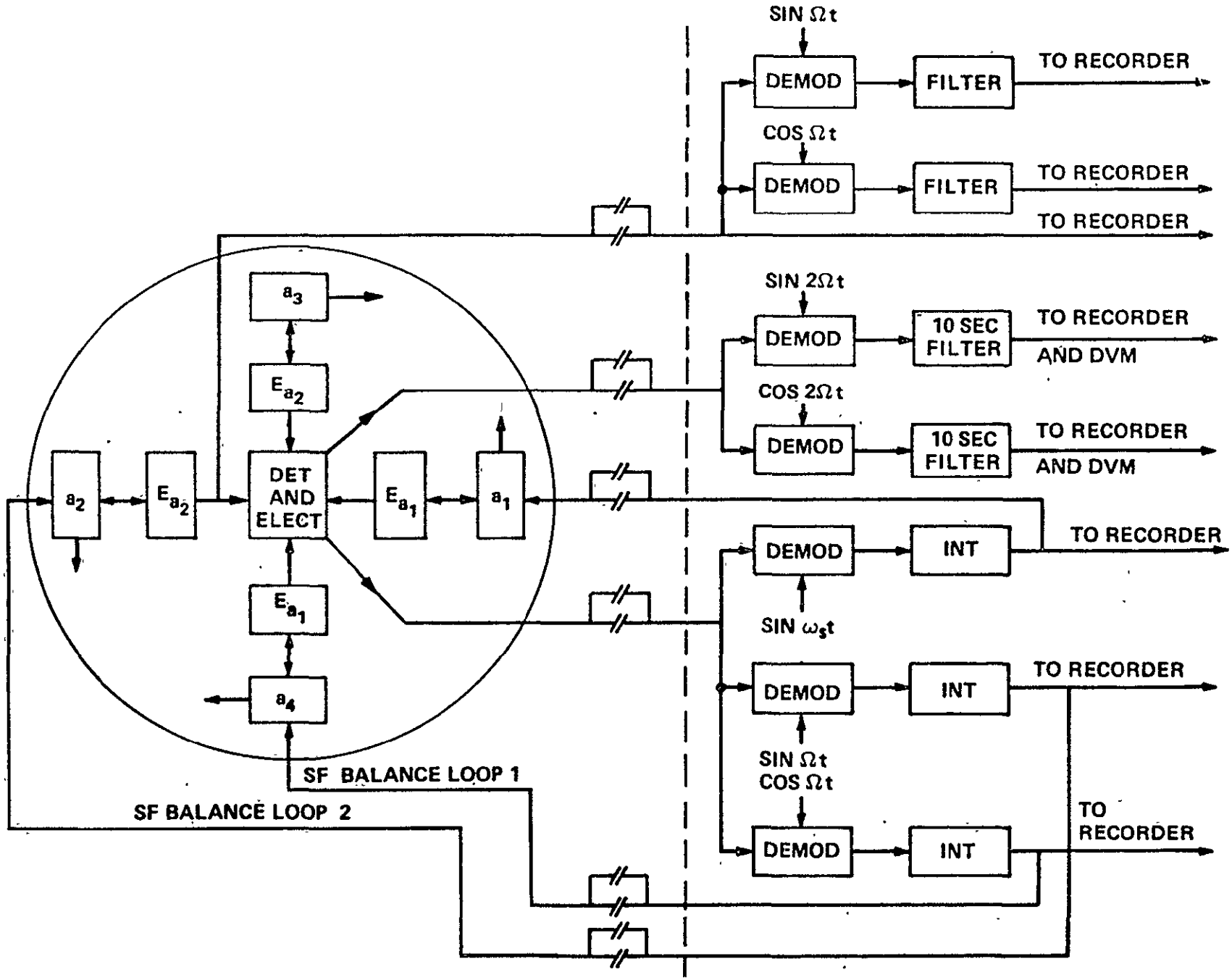

Figure 25. Block Diagram Rotating Accelerometer Gravity Gradiometer

ROTATING ACCELEROMETER GRAVITY GRADIOMETER

ROTATION SPEED: 3/8 Hz

OFF VERTICAL TILT OF ROTATION AXIS: APPROX 2 ARC MINUTES

DATA ACQUIRED: THROUGH DOUBLE SECTION 10 SEC FILTER RECORDED APPROXIMATELY EVERY 10 SEC

DATA ANALYZED: EVERY 128 DATA POINTS (APPROX 1280 SEC) 40 SEQUENTIAL BLOCKS OF DATA FOR BIAS, TREND AND 1σ RANDOMNESS BOTH GRADIOMETER CHANNELS

RESULTS:	1σ RANDOMNESS:	MEAN	80 DATA BLOCKS	1.07 EU
		WORST	80 DATA BLOCKS	1.27 EU
		BEST	80 DATA BLOCKS	0.87 EU
	BIAS: SINE CHANNEL -	MEAN	40 DATA BLOCKS	23.75 EU
		1σ DEV	40 DATA BLOCKS	0.39 EU
		TREND	40 DATA BLOCKS	2.2×10^{-3} EU/HR
	COS CHANNEL -	MEAN	40 DATA BLOCKS	7.54 EU
		1σ DEV	40 DATA BLOCKS	0.25 EU
		TREND	40 DATA BLOCKS	1.57×10^{-3} EU/HR

NOTE: APPROXIMATELY 100 EU BIAS BUCKED OUT BY PLACEMENT 100 KG M LEAD BALL

Figure 26. Performance Summary

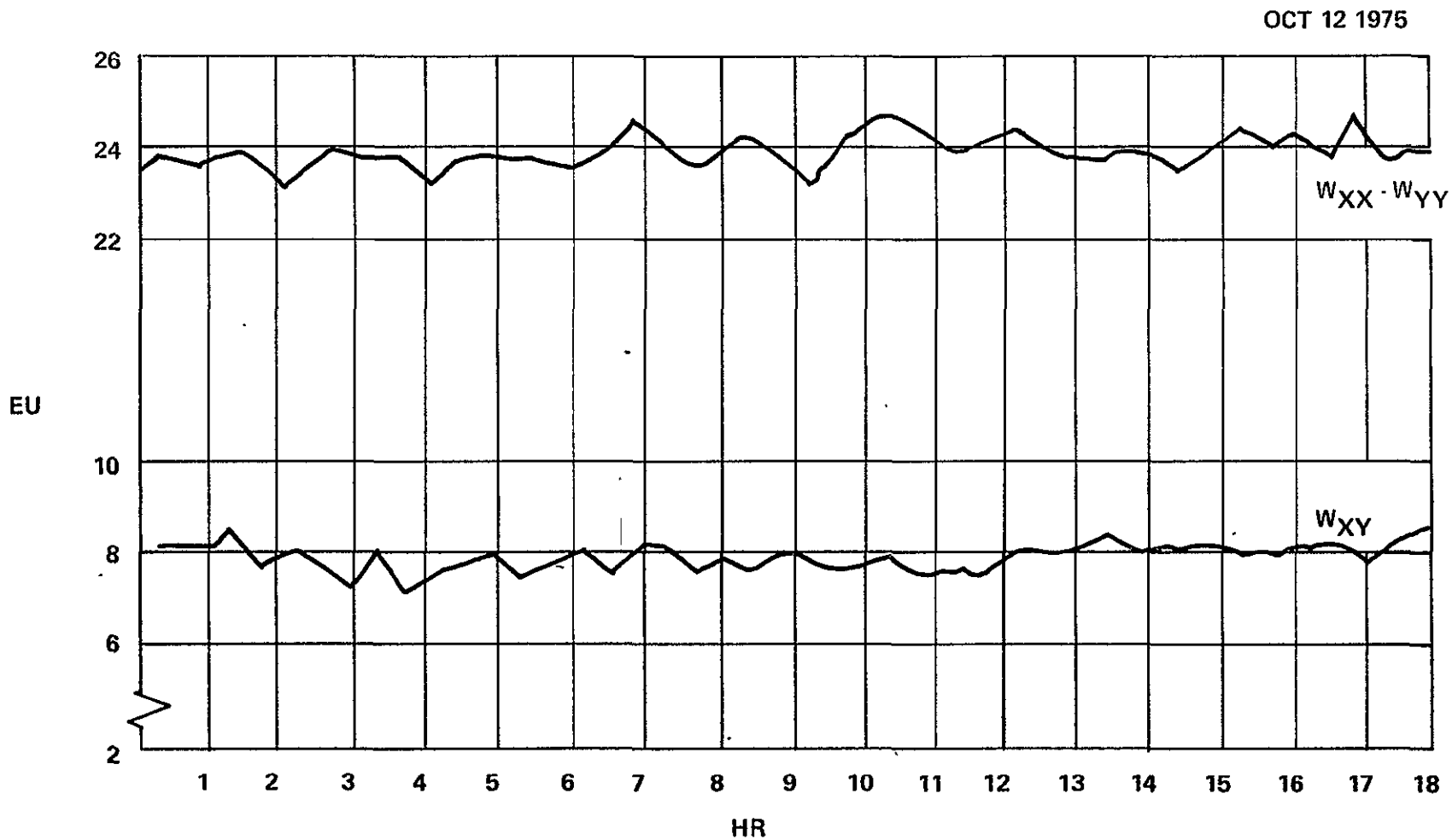

Figure 27. Rotating Accelerometer Gravity Gradiometer Stability Run 20 Minute Averages

The performance of the rotating accelerometer gravity gradiometer using Model VII accelerometers and the Holloman rate table is limited by the noise of the Model VIIs (non-rotating) which has been measured to be in the order of 0.9 EU and a small amount of additional noise introduced by the rate fixture.

The effectiveness of the common mode rejection of external disturbances using four Model VII accelerometers in combination with the automatic scale factor loops is clearly illustrated by the noise measured along the various axes of the Holloman rate table expressed in EUs as illustrated on Figure 28. The anticipation of being able to measure gradients to an accuracy of 0.03 EU is based on the use of the lower noise MESAs and the much smoother rotation provided by a spinning orbital vehicle.

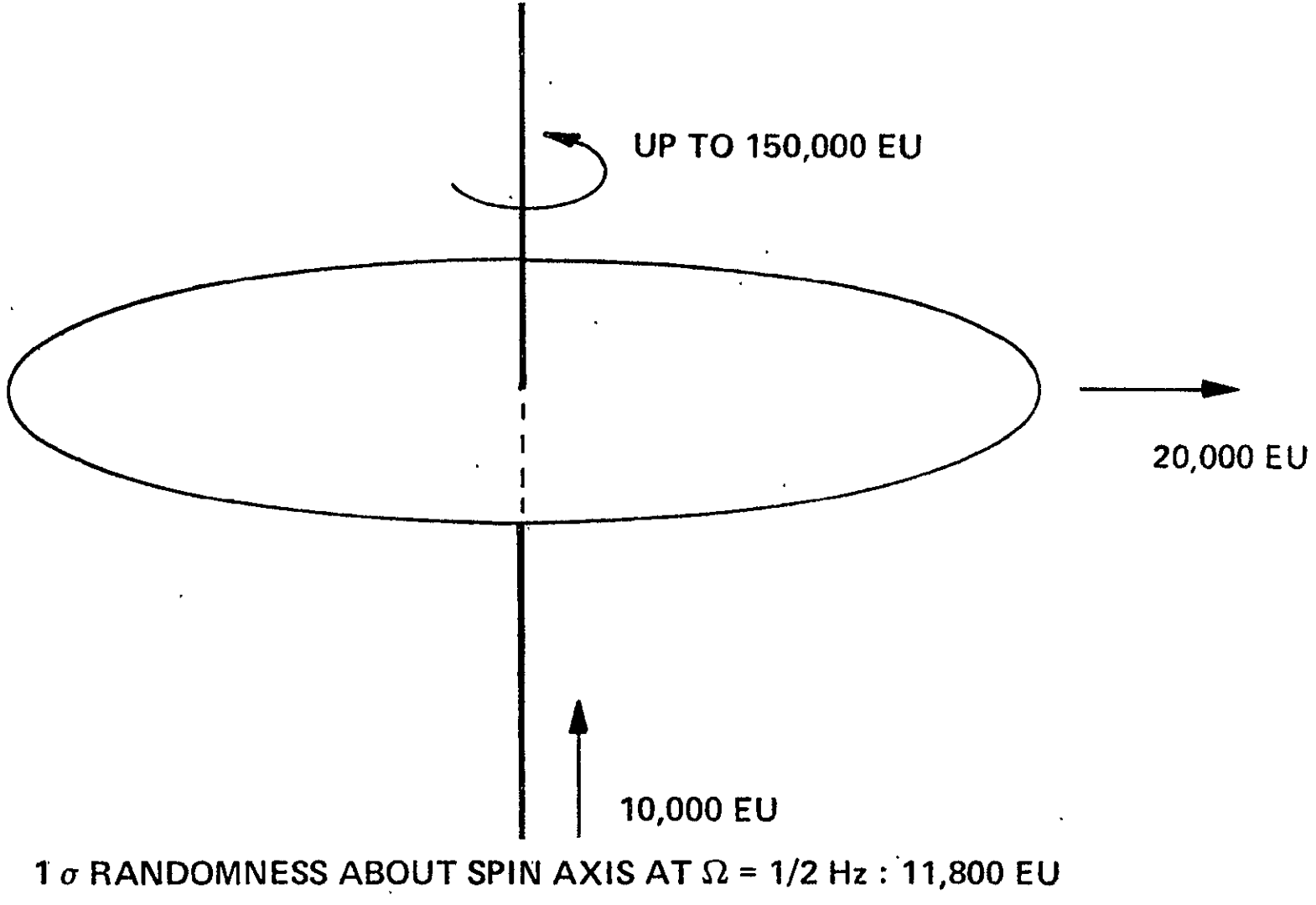

Figure 28. Nominal Amplitudes of 2Ω Experienced by a Sensor

6.0 CONCLUSIONS AND RECOMMENDATIONS

6.1 CONCLUSIONS

The following conclusions have been drawn based on this study.

- Gravity gradients to an accuracy of 0.03 EU in ten second average are possible with a slowly spinning orbital vehicle using four modified versions of the space qualified Miniature Electrostatic Accelerometer.

- At an orbital altitude of 300 km and a spin rate of 2 rpm, global gravity mapping to the 80 harmonic degree will be feasible with a 0.03 EU gravity gradient measuring accuracy.

- The spinning orbital gravity gradiometer self generates the demodulation reference and hence all signal processing to obtain the gradiometer outputs can be conducted onboard the satellite. Transmission of one 8-bit data point for the gradiometer channels every 15 seconds suffices for global gravity mapping and places only the most moderate requirements on data transmittal and handling. It is planned to buck out the nominal vertical gravity gradient of 4000 EU onboard the orbital vehicle.

- The attitude of the spin axis of the satellite should be maintained to 0.12 degrees in roll with respect to vertical to the orbital plane. Alternately knowledge of the roll attitude angle is satisfactory. The yaw attitude accuracy of the spin axis is not critical.

- Angular input rates about the yaw and roll axis should be under 1.10 deg/hr. Care will have to be exercised in the design of the space craft to avoid angular jitter induced by other equipment on the space craft from exceeding that rate. Attitude correction over the polar regions where much redundant data acquisition occurs is one option to be considered.

6.2 RECOMMENDATIONS

The two critical areas on which feasibility of an orbital gravity gradiometer depends are:

- The noise of the modified MESAs - The noise of a pair of MESAs modified for this application is readily tested in the laboratory and it is recommended that such a test program be conducted.

- The spinning orbital vehicle requirements are outlined in this report for the gravity gradiometer mission.

A review of a preliminary layout of the GRAVSAT with Fairchild and NASA Goddard personnel indicate it to be suitable for an orbital gravity gradient mission. A detail analysis with appropriate space craft engineering personnel is recommended to arrive at an optimum configuration for gravity gradient mission. An alternate possibility is a Scout Launcher vehicle. This should be explored further because of the potential cost effectiveness.

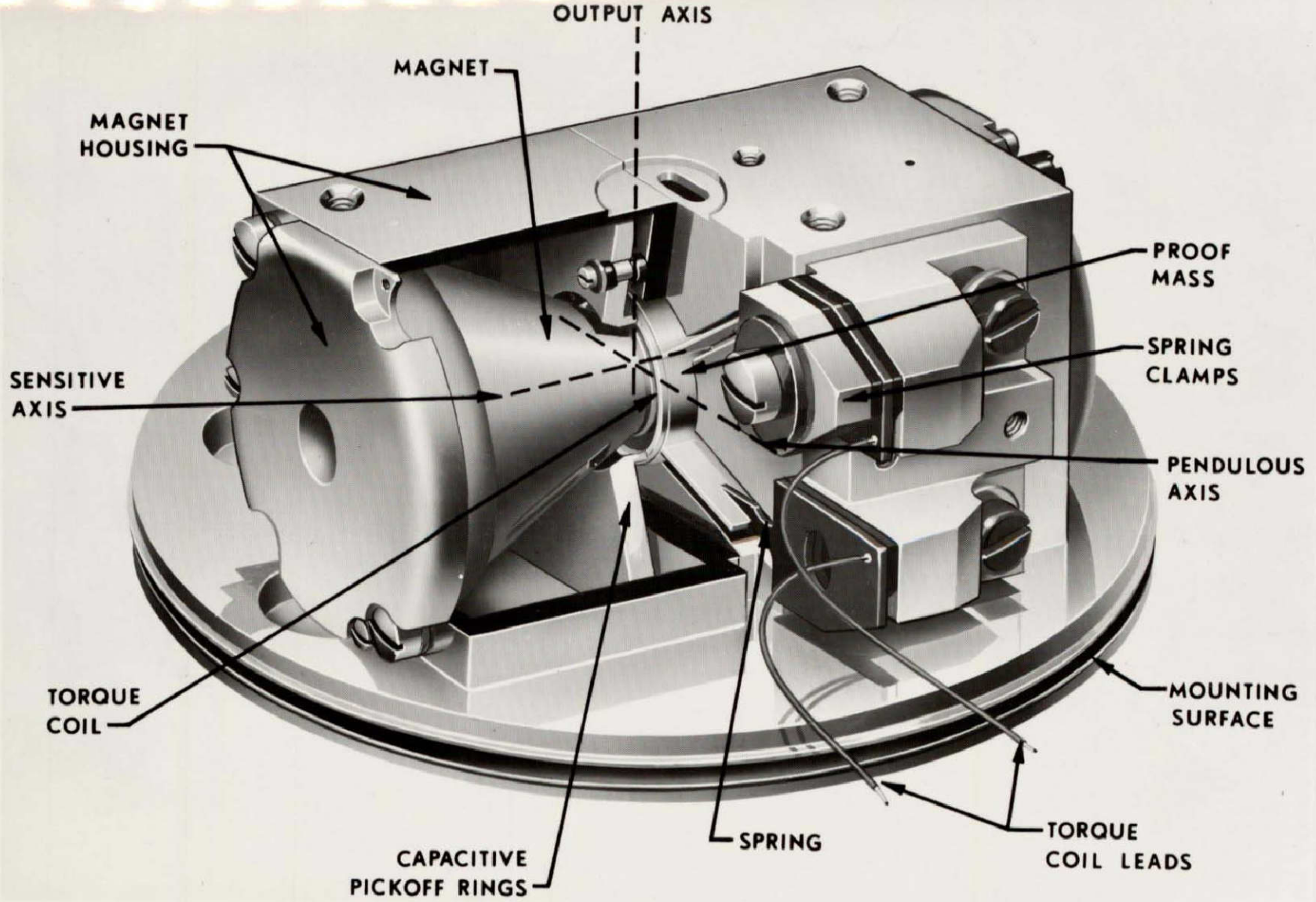
OUTPUT AXIS
MAGNET
MAGNET HOUSING
PROOF MASS
SPRING CLAMPS
SENSITIVE AXIS
PENDULOUS AXIS
TORQUE COIL
MOUNTING SURFACE
CAPACITIVE PICKOFF RINGS
SPRING
TORQUE COIL LEADS